# Precise measurement of $h/m_{\mathrm{Rb}}$ using Bloch oscillations in a vertical optical lattice: Determination of the fine-structure constant

Pierre Cladé,* Estefania de Mirandes, Malo Cadoret, Saïda Guellati-Khélifa,† Catherine Schwob, François Nez, Lucile Julien, and François Biraben

*Laboratoire Kastler Brossel, Ecole Normale Supérieure, CNRS, UPMC, 4 place Jussieu, 75252 Paris Cedex 05, France*

(Received 21 June 2006; published 21 November 2006)

Bloch oscillations in a frequency-chirped optical lattice are a powerful tool to transfer coherently many photon momenta to atoms. We have used this method to measure accurately the ratio $h/m_{\mathrm{Rb}}$. In this paper we detail the experimental procedure and we present a complete analysis of the different systematic effects. They yield a global relative uncertainty of 13 parts per $10^9$ (ppb). The measured value of $h/m_{\mathrm{Rb}}$ is $4.591\,359\,29\,(6)\times10^{-9}$ m$^2$ s$^{-1}$. The deduced value of the fine-structure constant is $\alpha^{-1}=137.035\,998\,84\,(91)$ with a relative uncertainty of 6.7 ppb.

DOI: 10.1103/PhysRevA.74.052109 PACS number(s): 06.20.Jr, 32.80.Pj, 32.80.Qk, 42.65.Dr

## I. INTRODUCTION

The fine-structure constant $\alpha$ is defined as

$$\alpha=\frac{e^2}{4\pi\epsilon_0\hbar c} \tag{1}$$

where $\epsilon_0$ is the permittivity of vacuum, $c$ is the speed of light, $e$ is the electron charge, and $\hbar=h/2\pi$ is the reduced Planck constant. The fine-structure constant sets the scale of the electromagnetic interaction, which is one of the four fundamental interactions. It appears and so can be determined in different domains of physics, which spread from atomic physics to mesoscopic and macroscopic condensed matter physics and elementary particle physics. The relevance of the fine-structure constant is that it is dimensionless, and therefore it does not depend on any unit system. Hence, this allows the comparison of all the various accurate measurements of $\alpha$, which constitutes an interesting test of the consistency of physics. This comparison is regularly made by the international Committee on Data for Science and Technology (CODATA), which determines the recommended values of all the physical constants from an adjustment of all the relevant data available [1]. One key weakness of the last adjustment made in 2002 is the lack of redundancy in the input data for $\alpha$. The estimation of this constant by CODATA2002 is essentially determined only by two data points, from the measurement of $h/m_{\mathrm{Cs}}$ where $m_{\mathrm{Cs}}$ is the atomic mass of cesium [relative uncertainty of 7.7 parts per $10^9$ (ppb)][2], and mainly by the electron magnetic moment anomaly $a_e$ (relative uncertainty of 3.8 ppb).

This situation has been modified recently: after almost two decades of work, a new experimental measurement of $a_e$ [3] along with an impressive improvement of the QED calculation [4] have led to a new determination of $\alpha$ with a relative uncertainty of 0.70 ppb. This important result renews the need of other determinations of $\alpha$ at the 1 ppb level for several reasons. (i) For the next CODATA adjustment, $\alpha$ will be mainly determined from only one measurement and this will be a true weakness. (ii) To test more stringently the QED calculations of $a_e$, an independent determination of $\alpha$ is needed. (iii) If we assume the accuracy of the QED calculation of $a_e$, another determination of $\alpha$ will give a limit upon the possible internal electron structure [5].

The recent proposal of a redefinition of the kilogram by fixing the value of the Planck constant $h$ [6,7] has also renewed the interest in having an accurate determination of the fine-structure constant. The realization of $h$ with the watt balance [7] relies on the validity of the expression $R_K=h/e^2=\mu_0 c/(2\alpha)$ where $R_K$ is the von Klitzing constant from the quantum Hall effect. At the present time there is a minor difference ($24\pm18$ ppb) between the determination of $\alpha$ deduced from $R_K$ [8] and the one deduced from the recent measurement of $a_e$ [5]. For a redefinition of the kilogram, a good alternative is to use the value of $\alpha$ issuing from the $a_e$ to define $R_K$, more accurately than it can be measured from the quantum Hall effect. In this case, it seems prudent to independently check the used value of $\alpha$ as accurately as possible.

In this paper, we report a determination of the fine-structure constant with a relative uncertainty of 6.7 ppb which is a first step toward a 1 ppb measurement. This experiment has the benefit of 20 years of research on atom-light interaction. Nowadays, laser cooling techniques enable a precise and easy control of the atomic motion [9]. Many applications of those techniques have been developed in metrology, such as the realization of microwave and optical clocks [10,11] or inertial sensors [12,13]. One of the earliest applications to the measurement of fundamental constants has been the determination of the fine-structure constant $\alpha$ using atom interferometry by Chu and co-workers [14]. This experimental determination of $\alpha$ is deduced from the measurement of $h/m_{\mathrm{Cs}}$ [2]. Indeed, the fine-structure constant can be related to the ratio $h/m_X$ [15] by

$$\alpha^2=\frac{2R_\infty}{c}\frac{A_r(X)}{A_r(e)}\frac{h}{m_X} \tag{2}$$

where $R_\infty$ is the Rydberg constant, $A_r(e)$ is the relative atomic mass of the electron, and $A_r(X)$ is the relative mass of

*Present Address: National Institute of Standards and Technology, 100 Bureau Drive, Stop 8424, Gaithersburg, MD 20899-8424.

†Also at: INM, Conservatoire National des Arts et Métiers, 61, rue Landy, 93210 La plaine Saint Denis, France.

 

the particle $X$ with mass $m_X$. These factors are known with a relative uncertainty of $7\times10^{-12}$ for $R_\infty$ [16,17], $4.4\times10^{-10}$ for $A_r(e)$ [18], and less than $2.0\times10^{-10}$ for $A_r$(Cs) and $A_r$(Rb) [19]. Hence, the factor limiting the accuracy of $\alpha$ is the ratio $h/m_X$.

In the present paper we report a determination of the fine-structure constant $\alpha$ deduced from the measurement of $h/m_{\mathrm{Rb}}$ [20]. The principle of the experiment consists in determining $h/m_{\mathrm{Rb}}$ through the accurate measurement of the rubidium recoil velocity $v_r=\hbar k/m_{\mathrm{Rb}}$ when the atom absorbs or emits a photon of wavevector $k$.

To determine precisely the recoil velocity, we transfer to the atoms a very high number of photon momenta without spontaneous emission and then we measure their velocity variation. The induced acceleration arises from a succession of stimulated two-photon transitions using two counterpropagating laser beams. Each transition modifies the atomic velocity by $2v_r$ leaving the internal state unchanged. This acceleration process can also be interpreted in terms of Bloch oscillations in the fundamental energy band of the periodic potential created by an optical standing wave. Bloch oscillations are a powerful tool to transfer to the atoms a very high number of recoil velocities in a short time with a high efficiency [21].

To measure accurately the atomic velocity variation, we prepare a narrow and well-determined initial velocity distribution. For this purpose we use two counterpropagating laser beams to induce a velocity-selective Raman transition. This first step defines the initial velocity class. After the acceleration process, the final atomic velocity is determined by measuring the Doppler effect by a second counterpropagating velocity-selective Raman transition. To determine the whole velocity profile the second Raman transition is scanned in frequency. The final uncertainty in the measurement of the recoil velocity $\sigma_{v_r}$ will therefore depend on two factors: (i) the uncertainty $\sigma_v$ of the *Raman inertial sensor* which measures the atomic velocity variation and (ii) the number $2N$ of photon momenta transferred to the atoms: $\sigma_{v_r}=\sigma_v/2N$.

The discussion is organized as follows. First, the Raman velocity sensor is described in Sec. II along with the noise sources which limit its sensitivity. Next, in Sec. III, we study the physical processus used to transfer to the atoms a high number of recoil velocities, i.e., Bloch oscillations in a frequency-chirped standing wave. In Sec. IV we present our experimental setup and in Sec. V our determination of the fine-structure constant. Finally, in Sec. VI we detail the systematic effects that limit the accuracy of $h/m_{\mathrm{Rb}}$ and $\alpha$.

## II. THE VELOCITY SENSOR

In this section we introduce the velocity sensor used to select and measure a narrow atomic velocity class. We also discuss the noise and error sources limiting the accuracy of the velocity sensor.

### A. Accurate selection and measurement of a narrow velocity class

The principle of the velocity sensor is described in Fig. 1. The main tool is the velocity-selective Raman transition between two hyperfine levels $|a\rangle,|b\rangle$ of the ground state, with energies $E_a$ and $E_b$. This transition is realized by using two counterpropagating laser beams with frequencies $\omega_1,\omega_2$ and wave vectors $\mathbf{k}_1,\mathbf{k}_2$. After the cooling process, the atoms are all in a well-defined internal state $|b\rangle$. We apply a first velocity-selective Raman $\pi$ pulse ($|b\rangle\rightarrow|a\rangle$) to define an initial velocity class centered on $v_i$. At resonance,

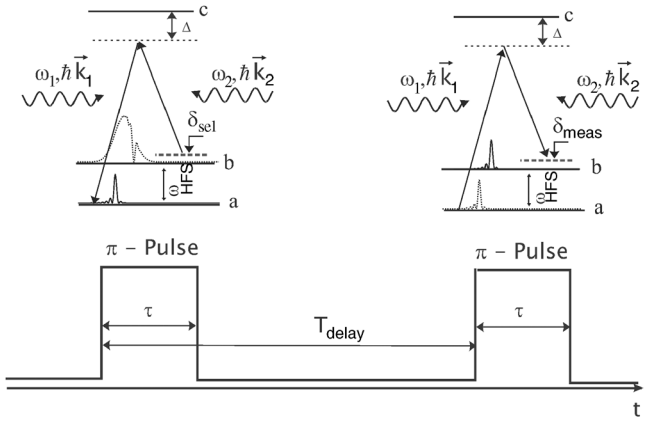


FIG. 1. Principle of the velocity sensor. The first Raman $\pi$ pulse drives a narrow velocity class of atoms from initial internal state $|b\rangle$ to state $|a\rangle$. The remaining atoms in $|b\rangle$ are pushed away. To measure the final velocity of atoms in $|a\rangle$ we use a second Raman $\pi$ pulse. This pulse transfers from $|a\rangle$ to $|b\rangle$ a velocity-dependent fraction of atoms.

$$\delta_{\mathrm{sel}}=\Delta_l+(\mathbf{k}_1-\mathbf{k}_2)\cdot\left(\mathbf{v}_i+\frac{\hbar}{2m}(\mathbf{k}_1-\mathbf{k}_2)\right) \tag{3}$$

where $\delta_{\mathrm{sel}}\equiv\omega_1-\omega_2-\omega_{\mathrm{HFS}}$ is the Raman detuning from the atomic resonance ($h\omega_{\mathrm{HFS}}=E_b-E_a$) and $\Delta_l$ is the differential shift of the atomic levels. This level shift takes into account a possible light shift and quadratic Zeeman level shifts. To cancel the associated systematic effects we use an experimental procedure described in the next section. The second term corresponds to the Doppler effect and to the atomic recoil. After this first step, we push away the remaining atoms in $|b\rangle$ by using a resonant beam tuned to the one-photon transition. Then an acceleration changes the atomic velocity from $v_i$ to $v_f$ (see Sec. III). Finally, to measure the final velocity, we apply a second $\pi$ pulse ($|a\rangle\rightarrow|b\rangle$) with a detuning $\delta_{\mathrm{meas}}$. To reconstruct the final velocity distribution, we repeat all the preceding steps by scanning the detuning $\delta_{\mathrm{meas}}$. The variation of velocity $\Delta\mathbf{v}$ is given by

$$\Delta\mathbf{v}\cdot(\mathbf{k}_1-\mathbf{k}_2)=(\delta_{\mathrm{meas}}^{\mathrm{max}}-\delta_{\mathrm{sel}}), \tag{4}$$

where $\delta_{\mathrm{meas}}^{\mathrm{max}}$ is the detuning at the maximum of the velocity distribution.

The final populations in both states $|a\rangle$ and $|b\rangle$ are measured by fluorescence using the time-of-flight technique (see Sec. IV). We emphasize that, even if the time-of-flight technique was initially developed for measuring the temperature of the cold atomic sample [22], we use this method only to extract information about the fraction of atoms in each hyperfine level.

As mentioned before, in such experiments, Raman transitions involve two hyperfine levels of the ground state. Therefore the width of the resonant velocity class $\Delta v$ is determined only by the photon coupling and the duration of the Raman pulse $\tau$. In particular, for a $\pi$ pulse

$$\Delta v \simeq \frac{1}{\tau(k_1+k_2)}. \tag{5}$$

As an example, for rubidium, $(k_1+k_2)v_r \simeq 15$ kHz, one selects an atomic velocity class of width $\Delta v \simeq v_r/15$ for $\tau = 1$ ms.

### B. Error sources and noise of the velocity sensor

Equation (3) shows that we have to control carefully the frequency difference between the two laser beams, $\omega_1-\omega_2$, and the differential atomic level shift $\Delta_l$ in order to ensure a good accuracy in the velocity measurement.

We are mainly concerned with two level shifts: light shifts and quadratic Zeeman shifts. In principle, level shifts are compensated between the selection and the measurement if they are induced by a constant field. However, there is a residual effect due to laser intensity fluctuations and spatial inhomogeneities of the magnetic field.

Nevertheless, the corresponding error in the determination of the recoil velocity changes sign when the direction of the Raman beams is reversed. Thus, the velocity is obtained from the mean value of two velocity measurements by exchanging the Raman beams. This idea is reflected by writing the resonance condition for the two configurations:

$$\delta = \Delta_l(z,t) - \epsilon_R(k_1+k_2)\left(v_i + \epsilon_R\frac{\hbar}{2m}(k_1+k_2)\right) \tag{6}$$

with $\epsilon_R = +1$ $(-1)$ for the configuration defined I (II) when the Raman recoil is upward (downward). From the two measurements of $\delta$, we obtain

$$\frac{\delta^{\mathrm{II}}-\delta^{\mathrm{I}}}{2} = \frac{\Delta_l(z^{\mathrm{II}},t^{\mathrm{II}}) - \Delta_l(z^{\mathrm{I}},t^{\mathrm{I}})}{2} + (k_1+k_2)v_i. \tag{7}$$

Assuming that both measurements take place at the same spatial point and that the magnetic field has a periodic dependence on the experimental sequence we have $\Delta_l(z^{\mathrm{II}},t^{\mathrm{II}}) \simeq \Delta_l(z^{\mathrm{I}},t^{\mathrm{I}})$. Hence, the atomic velocity can be written as

$$v_i = \frac{\delta^{\mathrm{II}}-\delta^{\mathrm{I}}}{2(k_1+k_2)}, \tag{8}$$

which is free from the systematic effect $\Delta_l(z,t)$.

The noise sources limiting the sensitivity of our velocity sensor have been widely studied in a previous paper [23]. At present, we are limited by the noise on the detection setup and the vibration noise of the retroreflecting mirror. The last can be reduced by an actively stabilized antivibration platform.

From all these considerations we are able to define the center of the atomic velocity distribution with a statistical uncertainty better than $v_r/10\,000$ in 5 min of integration time.

## III. COHERENT ACCELERATION OF THE ATOMS: BLOCH OSCILLATIONS

In this section we describe the physical process used to accelerate the atoms, transferring to them a well-defined number of recoil momenta by means of Bloch oscillations [24]. We also discuss some systematic effects that may arise from the modification of the velocity distribution of atoms in the optical lattice when we switch off the optical potential, and we justify the choice of a blue detuning for the Bloch laser beams.

### A. Atoms in a periodic optical potential

The atoms are coherently accelerated by using two counterpropagating laser beams, inducing a succession of two-photon Raman transitions. Each transition modifies the atomic velocity by $2v_r$, leaving the internal state unchanged. In order to compensate the Doppler shift the frequency difference of the two laser beams is linearly swept. A more suitable approach based on the Bloch formalism allows a more subtle description of the process: the interference of the two laser beams leads to a periodic light shift of the atomic energy levels. Thus, the atoms experience a periodic potential

$$U(x) = U_0 \cos^2(kx) \tag{9}$$

where $U_0 = \frac{\hbar\Gamma}{2}\frac{I}{I_s}\frac{\Gamma}{\Delta}$, $\Gamma$ being the natural width of the transition, $\Delta$ the detuning from the one-photon transition, $I$ the laser intensity of each beam, and $I_s$ the saturation intensity.

The periodicity of the potential leads to the well-known energy band structure, historically developed to describe the dynamics of electrons in a perfect crystal [25]. The Bloch theorem introduces two quantum numbers to solve this problem: $n$, the band index, and the wave vector $q$ (quasimomentum) which plays the same role in the motion of a particle in a periodic potential as the free-particle wave vector $p$ (true momentum) in the absence of any external potential.

The eigenstate solution of the corresponding Bloch Hamiltonian for a stationary periodic potential can be written in momentum space as

$$|\psi_{n,q}\rangle = |n,q\rangle = \sum_l \phi_n(q+2lk)|q+2lk\rangle \tag{10}$$

with $l \in \mathbb{Z}$. Here $|q\rangle$ designates the ket associated with a plane wave of quasimomentum $q$ and the amplitudes $\phi_n$ correspond to the Wannier function [26] in momentum space. From Eq. (10) we see that the only states coupled by the potential $U(x)$ are the plane waves with a momentum differing by a multiple of $2\hbar k$. The Wannier function $\phi_0$ for the fundamental energy band is shown in Fig. 2 for various potential depths $U_0/E_r$ ($E_r = \hbar^2k^2/2m$ is the recoil energy).

Now we consider a linear frequency chirp between the two laser beams $\Delta\omega(t)$. From the laboratory frame, the periodic potential $U(x)$ is now moving with a velocity $v(t) = \Delta\omega(t)/2k$. If $\Delta\omega(t)$ is adiabatically swept the atoms evolve in the same energy band, i.e., the fundamental band. The temporal evolution of the atomic wave function in momentum space is then given by

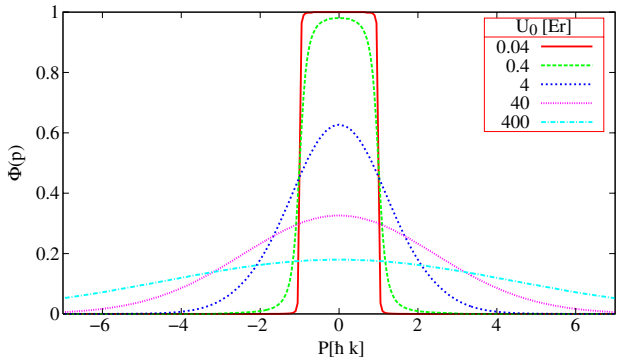


FIG. 2. (Color online) Wannier function in momentum space $\phi(p)$ for different potential heights $U_0$. When the potential depth is close to zero, the Wannier function is constant all over the first Brillouin zone and tends to 1.

$$|\Psi'(t)\rangle = \sum_l \phi_n[q(t) + 2lk]|q_0 + 2lk\rangle, \tag{11}$$

where $q_0$ is the quasimomentum associated with the center of the initial atomic velocity distribution and $q(t)=q_0+mv(t)/\hbar$. Consequently, only the enveloping Wannier function $\phi_n$ is time dependent. The atomic momentum distribution is periodic in time because it is described as the product of a Dirac comb with a time-translated envelope.

From the reference frame of the moving potential the atomic momentum distribution is now written as the product of a stationary enveloping Wannier function (centered in $q=0$) by a time-translated Dirac comb. Therefore $q(t)$ periodically scans the Brillouin zone giving rise to the well-known Bloch oscillations.

### B. Analysis of the final velocity distribution: Effect of the optical potential

In this section we discuss the displacement of the center of the final velocity distribution when the optical potential is switched off nonadiabaticaly. This effect was briefly described in a previous paper [27] where we presented a measurement of the Bloch oscillation frequency of atoms in a standing wave in the presence of a gravity field. In that experiment the effect induces a modification of the amplitude of the oscillations but does not give rise to a systematic effect in the Bloch frequency. This is not the case for the measurement presented in this paper.

We start from a selected narrow velocity class $\eta_{\rm sel}(p)$ centered around $p=0$. Then we load the atoms in the fundamental energy band $n=0$. By linearly chirping the frequency difference of the laser beams the atoms are made to perform $N$ Bloch oscillations, acquiring $2\hbar k$ per oscillation. At the end of this process if the potential is switched off in a sudden way, nonadiabatically, the final momentum distribution $\eta_{\rm fin}(p+2N\hbar k)$ can be obtained by projecting the atomic wave function $\Psi(t)$ in $p$ space. We find that the final momentum distribution, around the peak at $2N\hbar k$, is given by

$$\eta_{\rm fin}(p + 2N\hbar k) = |\phi_0(p + m\delta v)|^2 \eta_{\rm sel}(p) \tag{12}$$

where $\delta v$ is the difference between the average velocity of the cloud and the velocity of the optical lattice, i.e., the velocity of the cloud is $2Nv_r+\delta v$. The final distribution $\eta_{\rm fin}$ is given by the initial one $\eta_{\rm sel}$ modulated by the enveloping Wannier function $\phi_0(p)$. This leads not only to a reduction of the signal but also to a shift of the center of the distribution which depends on $\delta v$ (see Fig. 3). Let us estimate the corresponding systematic effect $\Delta_v$ in the measurement of the velocity. Assuming that the initial momentum distribution is $\Delta p \ll \hbar k$, one can develop $|\phi_0|^2$ to first order. Then Eq. (12) becomes

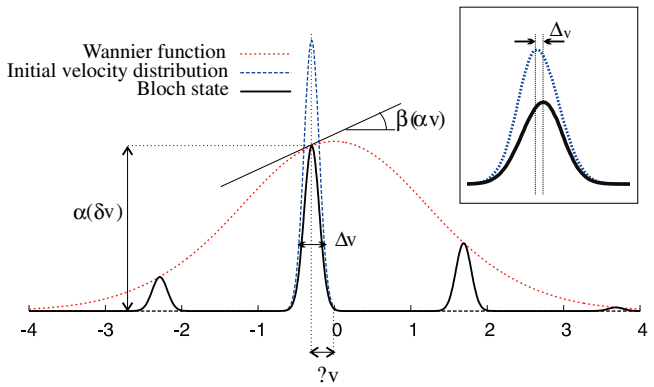


FIG. 3. (Color online) In this figure the envelope (dotted curve) corresponds to the Wannier function in momentum space $\phi_0(p)$. This function modulates the Bloch states (solid line). $\Delta v$ is the width of the velocity distribution and $\delta v$ is the difference between the atomic velocity and the center of the first Brillouin zone. $\alpha(\delta v)$ is the value of the Wannier function for a given $\delta v$ and $\beta(\delta v)$ is the derivative of the Wannier function normalized with respect to $v_r$. The inset is a zoom of the center of the Brillouin zone. It shows the shift $\Delta_v$ due to the Wannier function.

$$\eta_{\rm fin}(p + 2N\hbar k) = \left(\alpha(m\delta v) + \beta(m\delta v) \times \frac{p}{\hbar k}\right)\eta_{\rm sel}(p) \tag{13}$$

where $\alpha(v) \equiv |\phi_0(v)|^2$ and $\beta(v) \equiv v_r d\alpha/dv$.

Consequently, if the initial velocity distribution $\eta_{\rm sel}(p)$ is centered around $p=0$, the final velocity distribution $\eta_{\rm fin}(p)$ is not centered on $2N\hbar k$ but shifted by $m\Delta_v$ because of the first factor of Eq. (13) (see the inset of Fig. 3). Close to the maximum of $\eta_{\rm sel}(p)$ we obtain the following order of magnitude for this effect:

$$\frac{\Delta_v}{v_r} \propto \frac{\beta(\delta v)}{\alpha(\delta v)}\left(\frac{\Delta p}{\hbar k}\right)^2. \tag{14}$$

Figure 4 shows the numerical calculation of the ratio of coefficients $\beta/\alpha$ as a function of the potential depth $U_0$ for different values of $\delta v$. This ratio is maximal at the edge of the first Brillouin zone.

As an example, for a 1.2 ms $\pi$ pulse, with $U_0=10E_r$ and $\delta v=0.3v_r$, the systematic effect on the velocity measurement [evaluated from a numerical calculation of the coefficients of Eq. (14)] is about $7\times10^{-5}v_r$.

Instead, if the potential is adiabatically lowered, the Wannier function, which depends strongly on $U_0$ (see Fig. 2), tends to a square function over the first Brillouin zone and

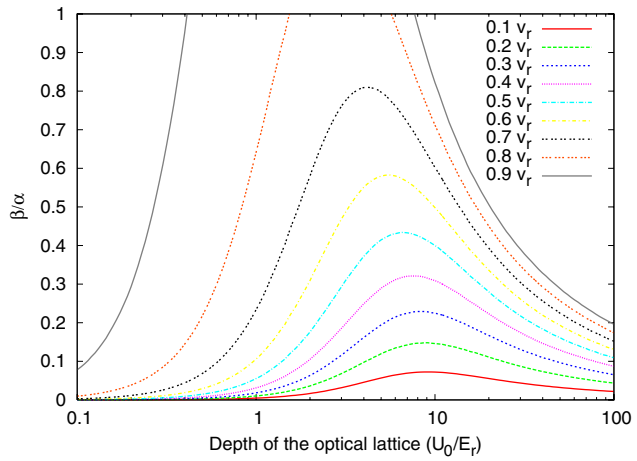


FIG. 4. (Color online) Numerical simulation of the ratio $\beta/\alpha$ versus the potential depth for different values of $\delta v$. This ratio increases fast when getting away from the center of the Brillouin zone.

thus $\alpha(v)\to 1$ and $\beta(v)\to 0$ for $|\delta v|\leqslant v_r$. No systematic effect in the measurement of the final velocity profile is then derived. Hence, in the experiment to determine $h/m_{\mathrm{Rb}}$ the optical potential has been switched off adiabatically.

### C. Choice of blue detuning of the potential to reduce spontaneous emission

In this section we discuss the effect of a red or a blue detuning $\Delta$ of the optical potential in the spontaneous emission rate. Indeed, spontaneous emission limits the number $N$ of Bloch oscillations the atoms are able to perform. Let us derive an expression comparing the rate of spontaneous emission for a red and a blue detuned potential. For our periodic potential (9) the spontaneous emission rate is given by

$$P_{\mathrm{sp}}(x) = \frac{U_0}{\hbar}\frac{\Gamma}{\Delta}\cos^2(kx). \tag{15}$$

In particular, for a Bloch state $|\Psi_{n,q}(x)\rangle$ the average spontaneous emission rate can be derived from $\langle\Psi_{n,q}(x)|P_{\mathrm{sp}}(x)|\Psi_{n,q}(x)\rangle$. One can write

$$\langle\cos^2(kx)\rangle = \frac{1}{2}c(U_0,q) \tag{16}$$

where $c(U_0,q)$ is a corrective factor which considers the beams' interference. Therefore,

$$c(U_0,q) = 1 + \langle\Psi_{n,q}(x)|\cos(2kx)|\Psi_{n,q}(x)\rangle. \tag{17}$$

In the tight-binding limit $|U_0|\gg E_r$, the atoms can be well described by particles trapped in a single lattice well. Let us now distinguish two cases: red and blue detuning of the potential.

#### *1. Red detuning of the potential, $\Delta<0$*

If $\Delta<0$, the atoms are trapped in the spatial region $x_0$ where the intensity of the field is the highest. Hence, we can approximate $\langle\cos(2kx)\rangle\simeq 1+\langle -2k^2x^2\rangle$ assuming $x_0=0$. To calculate $\langle -2k^2x^2\rangle$ we recall the expression of the mean value of a harmonic potential for the ground state $\langle -U_0k^2x^2\rangle = \frac{1}{2}\sqrt{|U_0|E_r}$. We find

$$c(U_0,q)_{\mathrm{red}} = 2 - \sqrt{\frac{E_r}{|U_0|}} \simeq 2. \tag{18}$$

We conclude that for a red detuning the atoms are led to the trap center seeking the highest field, and the spontaneous emission rate increases by a factor of 2 with respect to two noninterfering beams.

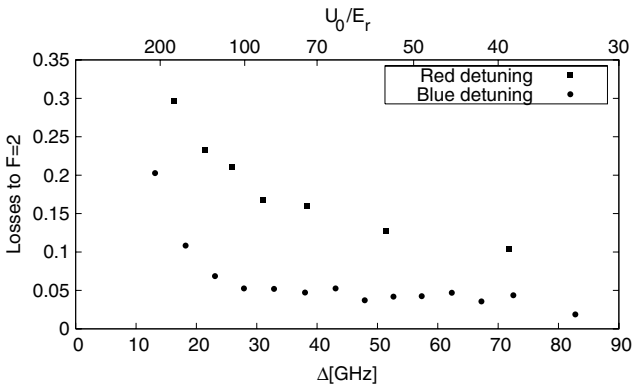


FIG. 5. Losses to $F=2$ induced by spontaneous emission versus the detuning $\Delta$. A blue detuning of the potential (circles) leads to fewer atomic losses than a red detuning (squares). As the intensities of the two Bloch beams are slightly different, the ratio between the losses (for red and blue detuning) does not verify the quantitative behavior predicted by the model described in this section.

#### *2. Blue detuning of the potential, $\Delta>0$*

If $\Delta>0$ the atoms are trapped at the spatial regions with minimum intensity. Therefore, the proper assumption now is $\langle\cos(2kx)\rangle\simeq -1+\langle +2k^2x^2\rangle$. An identical calculation as in the previous section leads to

$$c(U_0,q)_{\mathrm{blue}} = 1 + \langle\cos(2kx)\rangle = \sqrt{\frac{E_r}{|U_0|}}. \tag{19}$$

As a consequence, the ratio between the spontaneous rate in a blue-detuned lattice to that in a red-detuned one is

$$\frac{P^{\mathrm{blue}}}{P^{\mathrm{red}}} = \frac{1}{2}\sqrt{\frac{E_r}{|U_0|}}. \tag{20}$$

Notice that this result can also be expressed in terms of the Lamb-Dicke parameter $\eta$ [28], equal, in our case, to $(E_r/4U_0)^{1/4}$.

Hence, for $U_0\gg E_r$ a blue-detuned potential causes less spontaneous emission than a red-detuned one. These results have been confirmed by the following experiment (see Fig. 5). After the selection step we accelerate the atoms in $F=1$ during a given time. We evaluate the losses by measuring the fraction of atoms transferred to $F=2$ by spontaneous emission. As predicted, we see that a blue-detuned potential induces fewer losses than a red-detuned one. However, the

ratio between the losses (for red and blue detuning) does not verify the quantitative behavior predicted by Eq. (20). This is probably due to intensity imbalance between the two laser beams. The ratio of losses for a blue and a red detuning that we measure is about 4 compared to 10 expected by Eq. (20). This corresponds to an intensity imbalance of about 15% between the two laser beams.

### D. Effect of the transverse dipolar force on the width of the atomic velocity distribution

Up to now, we have neglected the atomic transverse degree of freedom. The finite size of the laser beams gives rise to a transverse dipolar force that pushes the atoms to (away from) the center of the beam in the case of red (blue) detuning. In the next paragraph we calculate this force and the associated acceleration focusing on the tight-binding regime and with a blue detuning of the potential.

We want to evaluate the potential energy $E(r)$ of an atom subjected to the potential $U(r,x)$ as a function of its distance $r$ from the propagation axis. We use a classical treatment for the transverse variable $r$ and the Bloch formalism for the propagation axis variable $x$. The optical potential can be written as

$$U(r,x) = U_0 \cos^2(kx) e^{(-2r^2/w_0^2)} \tag{21}$$

where $w_0$ is the beam waist. We consider an atom in the fundamental energy band. The average atomic energy is therefore

$$E(r) = U_0 e^{-2r^2/w_0^2} \langle \cos^2(kx) \rangle. \tag{22}$$

The transverse dipolar force is then

$$F = E_r \frac{2r}{w_0^2} \frac{U_0}{E_r} e^{(-2r^2/w_0^2)} c(U_0,q) \tag{23}$$

where $c(U_0,q)$ is defined in Eq. (17). In Sec. III D we showed that in the tight-binding regime and for a blue detuning of the potential $c(U_0) = \sqrt{E_r/|U_0|}$. Thus, the transverse acceleration for $r \ll w_0$ is given by

$$a_\perp = \frac{E_r}{m} \frac{2r}{w_0^2} \sqrt{\frac{|U_0|}{E_r}}. \tag{24}$$

As an example, for typical parameters $w_0 = 2$ mm and $r = 500$ $\mu$m, $a_\perp \simeq 4,3\sqrt{|U_0|/E_r}$ mm s$^{-2}$. For 10 ms of Bloch oscillations and $U_0 \simeq 100E_r$, we find a variation of the atomic transverse velocity of 0.43 mm/s $\approx v_r/10$. This shift is negligible compared to the spread of the transversal atomic velocity distribution. In conclusion, a blue detuning of the Bloch laser beams does not induce a significant transverse broadening of the atomic cloud.

## IV. EXPERIMENTAL SETUP

In this section we detail the experimental protocol and we present our results on the determination of the ratio $h/m_{\mathrm{Rb}}$ and the fine-structure constant $\alpha$ along with their statistical uncertainty.

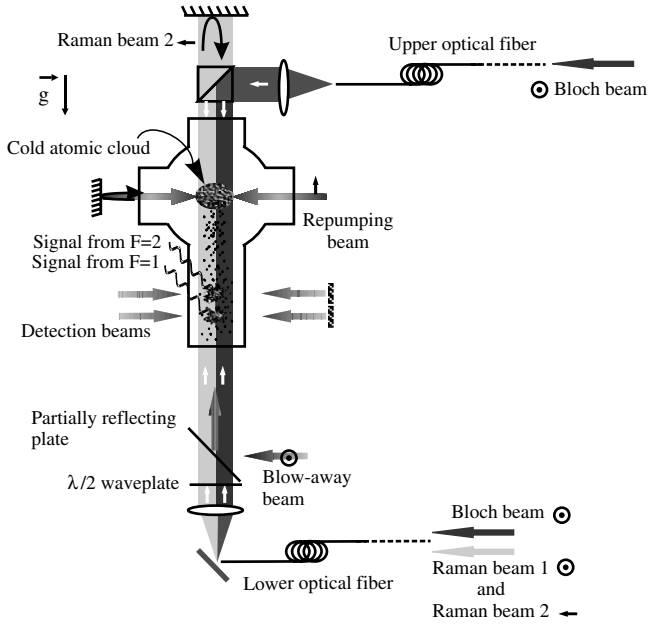


FIG. 6. Scheme of the experimental setup. The cold atomic cloud is produced in a MOT (the cooling laser beams are not shown). The Raman and the Bloch beams are in vertical geometry. The Raman beams and the upward Bloch beam are injected into the same optical fiber. The "blow-away" beam is tuned to the one-photon transition and allows us to clear the atoms remaining in $F=2$ after the selection step. The populations in the hyperfine levels $F=1$ and 2 are detected by fluorescence at 15 cm below the MOT using a time-of-flight technique.

The experimental sequence begins with the loading of a standard magneto-optical trap (MOT) from a rubidium vapor. After a few seconds the magnetic field is switched off and the atoms equilibrate in an optical molasses, reaching a temperature of 3 $\mu$K. Then the experiment develops in three steps: (i) we select a narrow subrecoil velocity class using a Raman velocity-selective $\pi$ pulse; (ii) we accelerate coherently the atoms by transferring to them $2N$ photon momenta by means of Bloch oscillations; (iii) we probe the final velocity distribution using another Raman $\pi$ pulse. Then we measure the proportion of atoms in the different hyperfine states (see Fig. 6). The Bloch and Raman beams are in vertical configuration. The detailed procedure is the following.

### A. Zeeman repumper

At the end of the optical molasses phase, $3\times10^7$ $^{87}$Rb atoms are in the $F=2$ state, equally distributed among all $m_F$ sublevels. In the experiment we address only the atoms in the $m_F=0$ state. Hence, to pump the atoms to $|F=2,m_F=0\rangle$, we shine during 50 $\mu$s a laser beam (Zeeman repumper) linearly polarized, parallel to the quantification axis, and resonant with the $F=2 \rightarrow F'=2$ transition. The Clebsch-Gordan coefficient for $|F=2,m_F=0\rangle \rightarrow |F'=2,m'_F=0\rangle$ is zero, so after many cycles the atoms will be optically pumped to the $|F=2,m_F=0\rangle$ state. The repumper beam increases the atomic

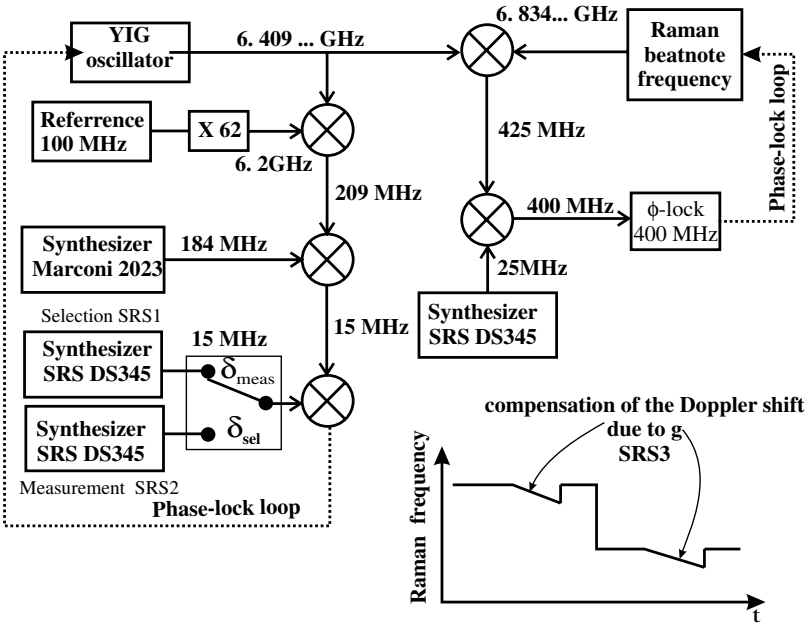


FIG. 7. Phase locking scheme for the Raman beams. The YIG oscillator is phase locked at 6.409 GHz by mixing it down with the 62nd harmonic of the quartz oscillator and with two synthesizers (Marconi 2030 and SRS DS345). All the synthesizers are referenced to the Cs clock. To perform the selection or the measurement, we switch between the two SRS DS345 synthesizers. A third SRS synthesizer is used to compensate the Doppler shift induced by the local acceleration of gravity.

fraction in the $|m_F=0>$ state, but it transfers momentum to the atoms, broadening the velocity distribution. Experimentally, the $|F=2,m_F=0\rangle$ density in momentum space increases by a factor of 2.

### B. Selection of a subrecoil velocity class

In order to select a narrow subrecoil velocity distribution we use a square counter-propagating Raman pulse in the lin $\perp$ lin configuration, with a frequency detuning fixed at $\delta_{\mathrm{sel}}$. A bias vertical magnetic field of 150 mG parallel to the propagation axis of the Raman beams is applied so that only the $m_F=0$ sublevel takes part in the Raman transition. The Raman pulse transfers atoms from the $5S_{1/2}|F=2,m_F=0\rangle$ to the $5S_{1/2}|F=1,m_F=0\rangle$ state. To reduce photon scattering and light shifts the Raman lasers are blue detuned by 1 THz from the $D2$ line. This detuning is chosen so that the Raman frequencies are close to the two-photon $^{85}$Rb standard [29]. For a power of 8 mW and a beam waist of 2 mm, the $\pi$ condition is achieved using a $\tau=3.4$ ms pulse. The width of the selected velocity class is $v_r/50$.

In order to reduce the phase noise, the two Raman beams follow the same optical path. They reach the lower part of the cell by the same fiber and to achieve a counterpropagating configuration one of them is retroreflected in the upper part of the cell. During the Raman pulse, the frequency of one Raman beam is linearly swept in order to compensate the Doppler shift induced by the fall of the atoms under the gravity field.

We generate the Raman beams by phase-locking two extended cavity diode lasers (ECLs). Their frequencies and phase difference are then referenced to a stable frequency source and can be controlled precisely. The beat note of the two overlapped beams ($f_{\mathrm{Raman}} \simeq 6.834$ GHz) is detected by a fast photodiode, amplified and mixed down with a local oscillator yttrium indium garnet (YIG) at a frequency $f_{\mathrm{YIG}} \simeq 6.409$ GHz to a more convenient intermediate frequency 425 MHz. This frequency is mixed with a frequency ramp around 25 MHz generated by a modulated synthesizer (SRS DS345). This ramp compensates the Doppler effect of the free-falling atoms and can be used for both the selection and the measurement (see Fig. 7). An adjustable band-pass filter keeps only the beat note at 400 MHz which is again divided by 4 and compared to the signal at 100 MHz from a referenced quartz. The frequency of this quartz is referenced to the Cs clock thanks to our optical fiber link with the Primary French Time Frequency Laboratory [30]. Their beat note is amplified once again and used as the input for three feedback paths. The fastest path acts directly on the diode. The second path uses the modulation input of the diode laser current controller. The slowest path uses a piezoelectric transducer to adjust the length of the ECL cavity.

The lasers are amplified in master-slave configurations with the slave being a high-power diode laser. Amplitude control of the laser light is achieved using 80 MHz acousto-optic modulators (AOMs) whose radio frequencies are also referenced to the same stable 100 MHz quartz oscillator. The frequencies of the Raman and Bloch beams are stabilized onto an ultrastable Zerodur® Fabry-Pérot cavity. We measure precisely one of the Raman beam frequencies by counting its beat note with a standard: the two-photon $5S_{1/2}(F=3)-5D_{1/2}(F=5)$ transition of $^{85}$Rb at $\nu_{2\mathrm{ph}}=385\,285\,142\,378(2)$ kHz [29,31] (see Fig. 8). From the beat note we can determine the Raman beam wavelength, the free spectral range of the cavity, and hence the Bloch beam wavelength. We use this optical reference to calibrate continuously the thermal drift of the cavity. The laser wavelengths can be thus determined with an uncertainty of 300 kHz.

### C. Push beam

After the Raman selection, the nonselected atoms remaining in $F=2$ are removed by a 3 ms laser pulse resonant with the $F=2\rightarrow F'=3$ transition. This beam is 6.8 GHz out of

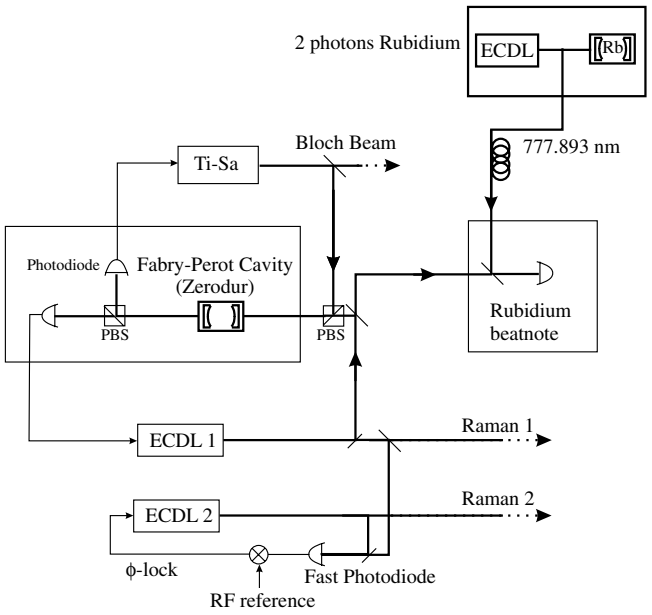


FIG. 8. Setup to stabilize and measure the Bloch and Raman beam frequencies. One of the Raman lasers and a Ti:sapphire laser are stabilized on a highly stable Fabry-Pérot cavity. Their frequencies are measured by counting the beat note with a two-photon Rb standard.

resonance from the atoms in $F=1$ and could exert a dipolar force on the Raman-selected cloud. To avoid this force the push beam is placed parallel to the Raman beams. Thus, the gradient of the dipolar force is transversal and there is no effect on the atom longitudinal velocity.

### D. Coherent acceleration

The optical lattice is the result of the interference of two counterpropagating laser beams in lin$\|$lin configuration. They are blue detuned by 40 GHz from the one-photon transition $5\,^2S_{1/2} \rightarrow 5\,^2P_{3/2}$. The optical lattice is raised adiabatically in 500 $\mu$s to load all the selected atoms in the fundamental Bloch band. The final potential depth is $70E_r$. In order to perform a coherent acceleration of the atoms, we sweep linearly in time the frequency difference between the two Bloch beams $\Delta\nu(t)$ using acousto-optic modulators: $\Delta\nu(t)=2at/\lambda$, where $a$ is the effective acceleration. In a 3 ms frequency sweep the atoms are accelerated at 1800 m s$^{-2}$ receiving 900 photon momenta. The efficiency per oscillation (taking into account spontaneous emission and nonadiabatic transitions) is 99.95%.

Finally, the lattice intensity is adiabatically lowered in 500 $\mu$s to bring the atoms back to a well-defined momentum state. Note that during the 500 $\mu$s of both adiabatic ramps, the optical lattice is constantly accelerated in order to compensate the gravity acceleration.

The Bloch lasers are produced by a Ti:sapphire laser pumped by a 10 W doubled neodymium-doped yttrium aluminum garnet laser at 532 nm (Millenia, Spectra Physics). The Ti:sapphire laser is frequency stabilized on the same Fabry-Pérot cavity used for the Raman beams. The output

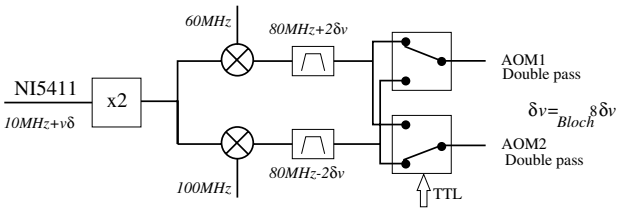


FIG. 9. Frequency control of the two AOMs for the Bloch beams.

power is 2 W with a tunability of some nanometers around 780 nm. The output is divided into two beams, each one controlled in frequency and amplitude by an independent AOM. The two beams reach the cell by two different fibers.

One of the Bloch beams is injected in the Raman beam fiber using the following trick. We place an AOM before the fiber and the Bloch beam is aligned into it with the AOM off while the first diffracted order of the Raman beams is aligned into the fiber with the AOM on. Hence, for each state of the AOM only one of the beams is selected into the fiber. The frequency difference between the Bloch beams is controlled by a frequency generator (NI5411) with a rate of $40\times10^6$ points per second. We program on it a frequency ramp around 10 MHz: $f(t)=10$ MHz$+\delta\nu(t)$. The output $f(t)$ is frequency doubled and divided into two paths (see Fig. 9). One path mixes the signal with 60 MHz coming from a synthesizer and the other path mixes it with 100 MHz from another synthesizer in order to obtain two opposite frequency ramps around 80 MHz to control each one of the Bloch AOMs and accelerate the atoms. As the AOM modulators are used in double-pass configuration, the acceleration of the lattice is then given by $a_{\text{lat}}=[8/(k_{B2}+k_{B1})]d\delta\nu/dt$ ($k_{B1}$ and $k_{B2}$ are the wave vectors of the Bloch beams). Using the frequency control scheme depicted in Fig. 9, the sum of these wave vectors does not vary at the first order during the acceleration process.

### E. Velocity measurement

After the coherent Bloch acceleration, we measure the final atomic velocity by means of a second Raman $\pi$ pulse with frequency $\delta_{\text{meas}}$. It transfers atomic population from $|F=1,m_F=0\rangle$ to $|F=2,m_F=0\rangle$ satisfying the relation (4). $\delta_{\text{meas}}$ is scanned in frequency in order to shape accurately the final velocity distribution. We are able to determine the center of the final distribution with an uncertainty on the order of 1 Hz, corresponding to about $7\times10^{-5}v_r$ in 10 min.

### F. Detection

The experimental method to detect the fraction of atoms in each hyperfine level ($F=1$ and $F=2$) recalls the one used in atomic clock systems [32]. We shine on the free-falling atoms at 15 cm below the trapping zone two parallel beams separated by 10 mm (see Fig. 10). The first one is a retroreflected circularly polarized laser beam resonant with the closed transition $F=2\rightarrow F'=3$ leaving the $F=1$ population unaffected. From the fluorescence signal in a photodiode we detect the atomic fraction in $F=2$. To avoid a decay in $F$

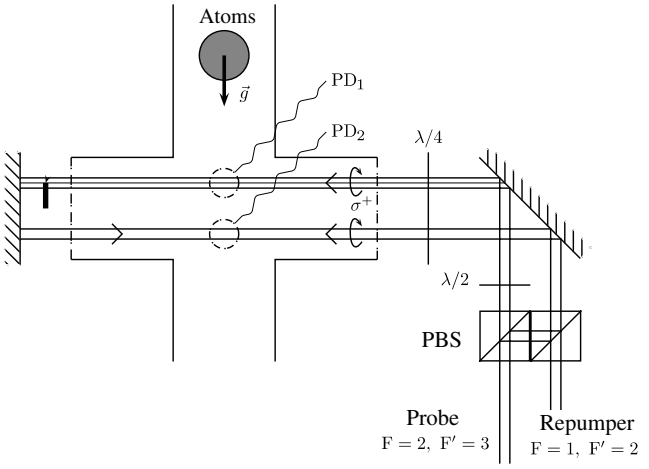


FIG. 10. Detection scheme.

=1 we add a magnetic bias field parallel to the detection beam propagation. Thus, the atoms will be quickly pumped to the $|F=2,m_F=2\rangle$ state. On the retroreflecting mirror of the first detection beam there is a small stain, which prevents the lowest part of the beam from coming back. In this way, the atoms detected in $F=2$ are subsequently pushed far away from the detection zone. The atomic fraction in $F=1$ continues to fall freely and is detected by the second laser beam placed below. This beam is a superposition of $F=2\rightarrow F'=3$ resonant light with a repumper beam resonant with the $F=1\rightarrow F'=2$ transition. The atoms in $F=1$ are hence pumped to the $F=2$ state and then detected following the previous procedure.

### G. Further improvements of the experimental protocol

The final sequence is strongly improved from the one described above in order to meet some experimental requirements and to reach a competitive uncertainty. The complete temporel sequence of both the intensity and the frequency of the different lasers is described in Fig. 11.

#### *1. Double acceleration*

After the Bloch acceleration, the atoms can reach the upper window of the vacuum chamber. To avoid it, we have implemented a double-acceleration scheme. At the end of the optical molasses phase, when all the atoms are in $F=2$, we effectuate a first acceleration of the cloud by means of $N_{\mathrm{first}}$ Bloch oscillations (see Fig. 11). The first Raman transition selects a narrow velocity class from the accelerated cloud. Then, the push beam eliminates the nonselected atoms. We apply the second acceleration, $N_{\mathrm{second}}$ Bloch oscillations, in the opposite direction to decelerate the atoms to $v\simeq 0$. Finally, the second Raman pulse measures the final velocity distribution. We emphasize that the velocity shift between the selection and the measurement is only due to the second Bloch acceleration, which is the one referred as "Bloch acceleration" everywhere in the text.

#### *2. Differential measurement and Raman beam inversion*

In this vertical configuration, we should know precisely the value of the local acceleration of gravity $g$ to measure

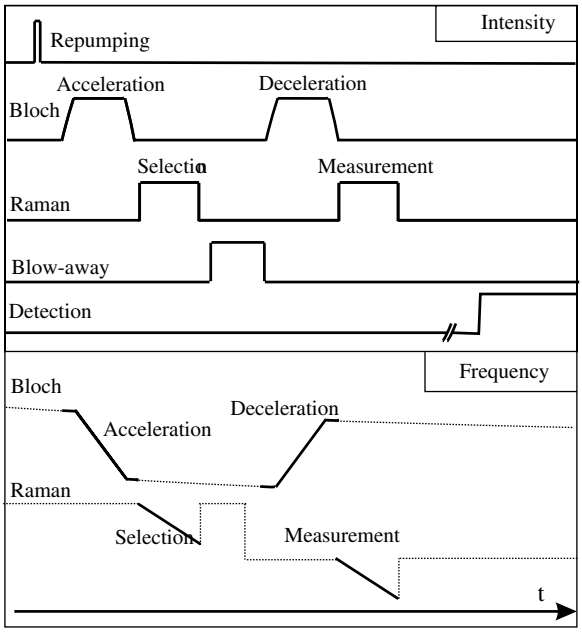


FIG. 11. Intensity and frequency timing of the different laser beams for the accerelation-deceleration sequence.

accurately the ratio $h/m_{\mathrm{Rb}}$. In order to cancel the effect of gravity we effectuate two identical measurements of $h/m_{\mathrm{Rb}}$ with opposite directions of the Bloch acceleration (up and down), keeping constant the delay between the selection and measurement $\pi$ pulses.[1] The ratio $\hbar/m_{\mathrm{Rb}}$ can be then determined from

$$\frac{\hbar}{m_{\mathrm{Rb}}}=\frac{(\delta_{\mathrm{sel}}-\delta_{\mathrm{meas}})^{\mathrm{up}}-(\delta_{\mathrm{sel}}-\delta_{\mathrm{meas}})^{\mathrm{down}}}{2(N^{\mathrm{up}}+N^{\mathrm{down}})k_B(k_1+k_2)} \tag{25}$$

where $N^{\mathrm{up\ down}}$ correspond, respectively, to the number of Bloch oscillations in the two opposite directions, $k_B$ is the Bloch wave vector, and $k_1$ and $k_2$ are the wave vectors of the two Raman beams.

As discussed in Sec. II, the contribution of some systematic effects to the determination of $h/m_{\mathrm{Rb}}$ changes sign when the direction of the Raman beams is exchanged (see Fig. 12). Hence, for each up or down trajectory when the Raman beams are reversed, we record two velocity spectra, and we take the mean value of these two measurements. Finally, each determination of $h/m_{\mathrm{Rb}}$ and $\alpha$ is obtained from four velocity spectra (see Fig. 13).

## V. EXPERIMENTAL RESULTS. DETERMINATION OF $h/m_{\mathrm{Rb}}$ AND THE FINE-STRUCTURE CONSTANT

Here we present our final determinations of $h/m_{\mathrm{Rb}}$ and $\alpha$. They have been derived from 72 experimental data point taken during four days.

Each determination of $h/m_{\mathrm{Rb}}$ is obtained from four spectra as detailed in the previous section. Each spectrum contains 160 points and is obtained in 5 min. The uncertainty in

[1]We emphasize that neither the trigger generator nor the synthesizer making the sweep to compensate $g$ is reprogrammed.

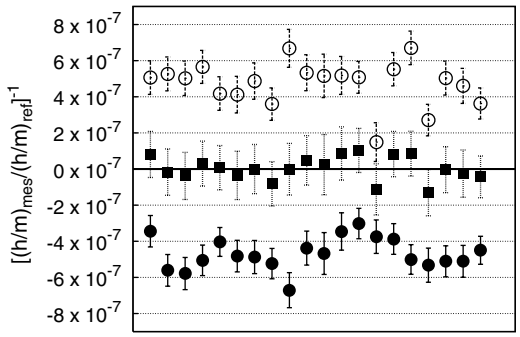


FIG. 12. $h/m_{\mathrm{Rb}}$ measurements are obtained by inverting the Raman beams (circles). $B \simeq 150$ mG. The mean value of each pair of measurements (squares) cancels out systematic effects, such as light shifts and quadratic Zeeman shifts. For clarity, we plot the ratio of the measured $(h/m)_{\mathrm{meas}}$ to $(h/m)_{\mathrm{ref}}$, where $(h/m)_{\mathrm{ref}}$ is the value derived from $\alpha_{2002}$.

the determination of the central frequency of each spectrum is about 1.7 Hz ($\simeq 10^{-4} v_R$). We show in Fig. 13 four typical velocity distributions for $N^{\mathrm{up}}=430$ Bloch oscillations and $N^{\mathrm{down}}=460$ oscillations. The effective recoil number is here $2(N^{\mathrm{up}}+N^{\mathrm{down}})=1780$.

In Table I we present the parameters for the Bloch and Raman beams in all our determinations of $\alpha$.

The parameters of the four spectra of each measurement are summarized in Table II, where $N_{\mathrm{first}}$ and $N_{\mathrm{second}}$ are the numbers of Bloch oscillations in the acceleration-

TABLE I. Power, intensity, and detuning of the Bloch and Raman beams in the measurements.

| | Raman beams | Bloch beams |
|---|---|---|
| $P$ | 10 mW | 115 mW |
| $I$ | 150 mW/cm$^2$ | 180 mW/cm$^2$ |
| Detuning | 1 THz | 40 GHz |

deceleration process of each measurement of $h/m_{\mathrm{Rb}}$. The sign of $\epsilon_R$ represents the inversion of the Raman beams.

Figure 14 presents the set of 72 determinations of the fine-structure constant $\alpha$. In each one of them, we have transferred to the atoms up to 460 Bloch oscillations, with an efficiency of 99.95% per oscillation. Each determination is obtained after 20 min of integration time. The corresponding relative uncertainty in $h/m_{\mathrm{Rb}}$ is around $6.6\times10^{-8}$ and hence $\alpha$ is deduced with a relative uncertainty of $3.3\times10^{-8}$. The dispersion of these $n=72$ measurements is $\chi^2/(n-1)=1.3$ and the resulting statistical relative uncertainty on $h/m_{\mathrm{Rb}}$ is 8.8 ppb.

The experimental value of $h/m_{\mathrm{Rb}}$, taking into account only the statistical uncertainty, without any correction, is for the isotope $^{87}$Rb

$$\frac{h}{m_{\mathrm{Rb}}} = 4.591\ 359\ 237(40) \times 10^{-9}\ \mathrm{m^2\ s^{-1}} \quad [8.8 \times 10^{-9}] \tag{26}$$

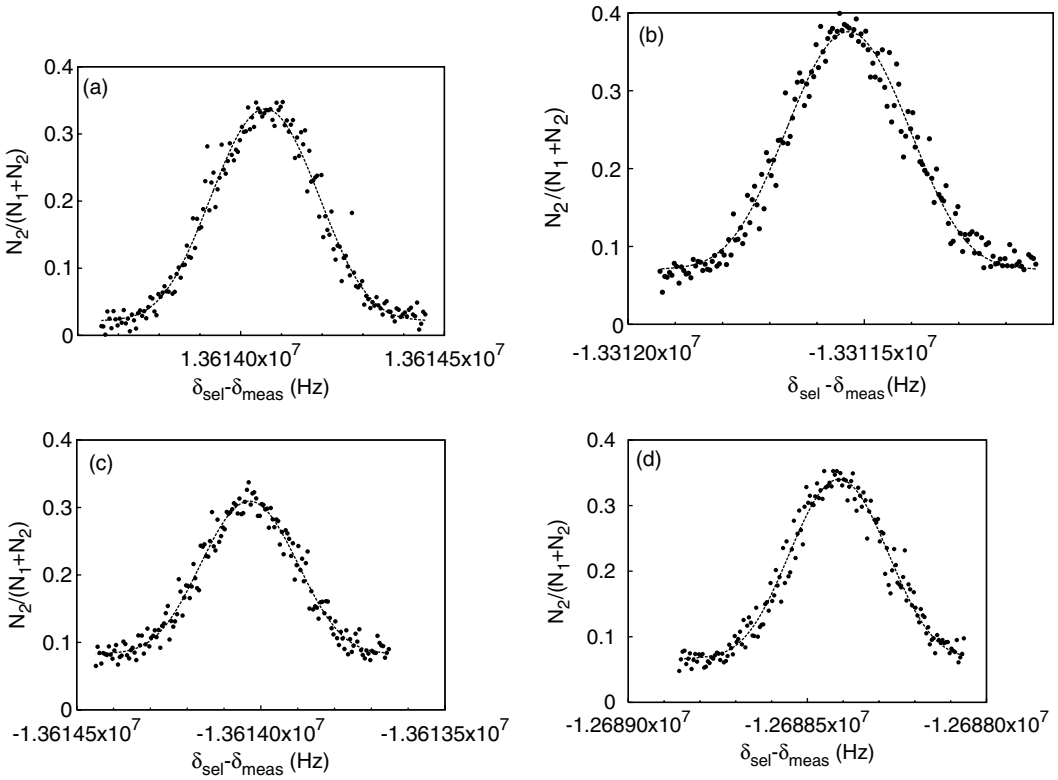


FIG. 13. Sequence of four spectra used for each determination of $\alpha$. Here $N_1$ and $N_2$ are, respectively, the numbers of atoms in $F=1$ and $F=2$ after the acceleration process. They are obtained by exchanging the Raman beam directions and performing the Bloch acceleration upward or downward. The parameters used for each spectrum are summarized in Table II. The relative uncertainty for each spectrum is about 1.7 Hz. From the four spectra, $h/m_{\mathrm{Rb}}$ can be determined with an uncertainty of $6.6\times10^{-8}$.

TABLE II. Parameters of the four spectra used for each determination of $\alpha$. $N_{\mathrm{first}}$ and $N_{\mathrm{second}}$ are defined in Sec. (IV G 1).

| | Spectrum 1 | Spectrum 2 | Spectrum 3 | Spectrum 4 |
|---|---|---|---|---|
| $N_{\mathrm{first}}$ | −450 | 390 | −450 | 390 |
| $N_{\mathrm{second}}$ | 460 | −430 | 460 | −430 |
| $\epsilon_R$ | −1 | −1 | 1 | 1 |
| $\nu_{\mathrm{sel}}$ (Hz) | −13956985 | 11455931 | 13926651 | −11486265 |
| $\nu_{\mathrm{meas}}$ (Hz) | −342932 | −1855606 | 312598 | 1825272 |

The deduced value of $\alpha^{-1}$ is then

$$\alpha^{-1} = 137.035\ 999\ 59(60) \quad [4.4 \times 10^{-9}]. \tag{27}$$

In the next section, all systematic effects affecting the experimental measurement will be analyzed and taken into account to determine the final values of $h/m_{\mathrm{Rb}}$ and $\alpha$.

## VI. SYSTEMATIC EFFECTS

In this section we present the different systematic effects limiting the measurement of the ratio $h/m_{\mathrm{Rb}}$ and the associated uncertainties. The resulting relative uncertainty on the fine-structure constant is derived.

### A. Wave-front curvature and Gouy phase

The relation $p=h\nu/c$ for the impulsion of a photon as a function of its frequency is only valid for a plane wave. In the more realistic case of a beam of finite waist, there are corrections to this relation which can be characterized by the Gouy phase shift [33] and the wave-front curvature. We evaluate these two corrections in the same formulas as a function of the beam's parameters.

Let us first calculate an order of magnitude of the Gouy phase shift. The Gouy phase is the phase describing the $\pi$ phase shift at the focus of a beam. The laser beam can be described as a sum of plane waves, and the Gouy phase shift is due to the dispersion of the **k** wave vectors. Each wave vector has a component along the propagation axis ($k_z$) and a component orthogonal to this axis ($k_\perp$). Each plane wave has the same frequency, so we have the relation $k^2=\omega^2/c^2=k_z^2+k_\perp^2$. For a beam of minimal waist $w_0$, the dispersion in $k_\perp$ is Fourier limited to $1/w_0$. At the position of the minimal waist, where all the plane waves are in phase, the wave vector is of the order of

$$k_z = \sqrt{k^2 - k_\perp^2} \simeq k\left(1 - \frac{k_\perp^2}{2k^2}\right). \tag{28}$$

The correction is thus of the order of $1/k^2w_0^2$. The effect of the Gouy phase shift is to reduce the effective wave vector. This effect is very similar to the reduction of the speed of an electromagnetic wave confined in a wave guide. On the other hand, the conservation of momentum implies that a beam passing through a lens (and then having a different waist $w_0$) will exert onto it a force. This force has been in fact known for a long time and it is used, for example, for trapping dielectric particle in optical tweezers [34].

In order to calculate the exact effect at a position $z$ from the minimal waist and $r$ from the axis, we have to take into account the phase between the different plane waves interfering at that point. This will lead to the Gouy effect (dependence upon $z$) and the wave-front curvature (dependence upon $r$). The effective wave vector resulting from the interference of each plane wave can also be directly obtained from the gradient of the phase of the laser beam [35]:

$$k_z^{\mathrm{eff}} = \frac{d\phi}{dz} = k - \frac{2}{kw(z)^2}\left(1 - \frac{r^2}{w(z)^2}[1-(z/z_R)^2]\right) \tag{29}$$

where $z_R=\pi w_0^2/\lambda$ is the Rayleigh length and $w(z)^2=w_0^2[1+(z/z_R)^2]$. Notice that at $z=z_R$, where the wave-front curvature is maximal, the effective wave vector does not depend upon $r$.

Equation (29) gives the effective wave vector as a function of two parameters: $w(z)$, the waist of the beam at the measurement point, and $z/z_R$. To evaluate these two parameters, we have used a Shack-Hartmann wave-front analyzer (HASO 64, Imagine Optic) which measures the wave-front curvature radius $R(z)$ and the waist $w(z)$ at a given position. Assuming that our beam is a Gaussian beam, and thus using the relation $R(z)=z[1+(z_R/z)^2]$, we obtain that

$$\frac{z}{z_R} = \left(\frac{\pi}{\lambda}\frac{w(z)^2}{R(z)}\right). \tag{30}$$

The wave-front curvature effect depends upon the distance $r$ from the propagation axis. To calculate the effect, we need to know the mean value of $r^2$. The diameter of the atomic cloud measured using absorption imaging is $\langle r^2 \rangle$

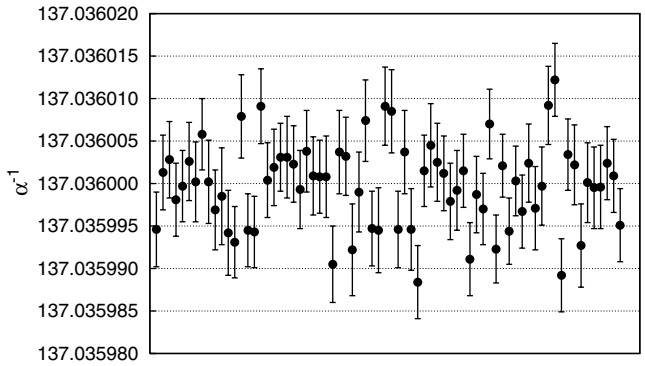


FIG. 14. Chronologically, our 72 determinations of the fine-structure constant.

TABLE III. Wave-front parameters of the Raman and Bloch laser beams.

| | $w(z)$ (mm) | $R(z)$ (m) | $k_z^{\text{eff}}/k-1$ (ppb) |
|---|---|---|---|
| Upward beams | 2.1 | 15.9 | −7 |
| Bloch (downward) | 2.0 | 7.0 | −14 |
| Raman (downward) | 2.4 | 31.6 | −5 |

$\simeq(800\ \mu\text{m})^2$. The light beams were centered on the atomic cloud by using copropagating Raman transitions and maximizing the number of transferred atoms. We estimate that the cloud is in the center of the Raman beams with a precision better than 500 $\mu$m, leading to $\langle r^2\rangle \simeq (950\ \mu\text{m})^2$.

Table III gives the wave-front parameters of the different beams involved in our experiment. Using the fact that $h/m_{\text{Rb}} \propto (k_R k_B)^{-1}$ [see Eq. (25)], where $k_R$ and $k_B$ are the mean values of the effective wave vector for the Raman and the Bloch beams, the final relative correction on $h/m_{\text{Rb}}$ is 16.4 ppb. The uncertainty of the measured wave-front curvature is quite high. We thus took a conservative uncertainty of 50%, leading to a relative uncertainty of 8 ppb.

### B. Laser beam alignment

In Eq. (25) we supposed that both Raman and Bloch beams are counterpropagating. Rigorously, one should replace the term $2k_B(k_1+k_2)$ by $(\mathbf{k}_R^U-\mathbf{k}_R^D)\cdot(\mathbf{k}_B^U-\mathbf{k}_B^D)$, where $(\mathbf{k}_R^U,\mathbf{k}_R^D)$ and $(\mathbf{k}_B^U,\mathbf{k}_B^D)$ are, respectively, the wave vectors of the Raman and the Bloch beams defined in Fig. 15. The two

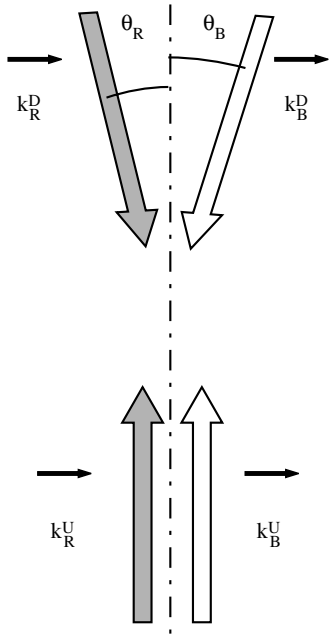


FIG. 15. Laser beam alignment. In our geometry, the two upward propagating beams come from the same fiber and thus are parallel. We denote by $\theta_R$ ($\theta_B$) the angle between the two Raman (Bloch) beams.

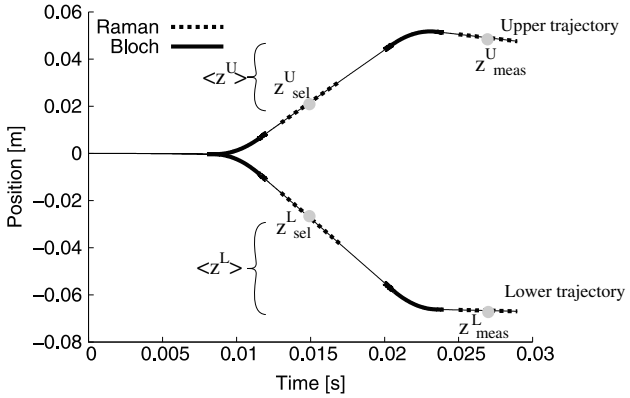


FIG. 16. Position of atoms for the upper and lower trajectories.

upward-propagating wave vectors are parallel because the beams come out from the same fiber. The correction to apply will then depend only upon the angles $\theta_R$ and $\theta_B$ between the upward and downward Bloch and Raman beams (see Fig. 15). If all four wave vectors are in the same plane, and in the limit $\theta_R$ and $\theta_B \ll 1$, the relative correction to $h/m_{\text{Rb}}$ is given by $(\theta_B^2+\theta_R^2-\theta_B\theta_R)/4$.

The alignment of the counterpropagating beams was done by maximizing the coupling of the downward-propagating beams into the lower fiber. For the Raman beam, we measured a reduction of the coupling by a factor of 2 when we tilted the mirror by $7\times10^{-5}$ rad. Assuming that the coupling was within 10% of the optimum, we find $\theta_R \approx 3\times10^{-5}$ rad. Similarly, $\theta_B \approx 1.6\times10^{-4}$ rad for the Bloch beam.

In the worst case where $\theta_B$ and $\theta_R$ have opposite signs, we obtain a systematic effect of $8\times10^{-9}$. Thus, we assume a relative systematic effect on $h/m_{\text{Rb}}$ of $4\times10^{-9}$, with a relative uncertainty of $4\times10^{-9}$.

### C. Gravity gradient

The local acceleration of gravity $g$ induces an atomic velocity variation of $gT_{\text{delay}}$, where $T_{\text{delay}}$ is the time between the selection and measurement pulses. However, to cancel the effect of this velocity shift we use the same temporal sequence for the upper and lower atomic trajectories. Nevertheless, gravity will be slightly different for the two trajectories because of the gravity gradient $\partial_z g$ (see Fig. 16). The atomic velocity variation due to this gradient is then proportional to the mean value of $z$ during the flight. The correction on $h/m_{\text{Rb}}$ is thus

$$\frac{m_{\text{Rb}}}{h}\Delta\left(\frac{h}{m_{\text{Rb}}}\right)_{\text{grav. grad.}} = \frac{T_{\text{delay}}(\langle z\rangle^U - \langle z\rangle^L)\partial_z g}{2v_r(N^{\text{up}}+N^{\text{down}})}, \qquad (31)$$

where $\langle z\rangle^U-\langle z\rangle^L$ is the difference between the mean positions of the upper and lower trajectories (see Fig. 16) and $N^{\text{up}}+N^{\text{down}}$ is the total number of Bloch oscillations done for the two trajectories. We calculate $\langle z\rangle^U-\langle z\rangle^L=10$ cm. The gravity gradient is, neglecting effects due to earth rotation, $\partial_z g=-2g/R_T\simeq 3.1\times10^{-7}g\ \text{m}^{-1}$ ($R_T$ is the radius of the earth). With $T_{\text{delay}}=12$ ms, we obtain a relative correction for $h/m_{\text{Rb}}$ of $3.6\times10^{-10}$ (for coherence with Table V.

TABLE IV. Refractive index for the different steps of the experiment.

| | Detuning | $\rho$ (atoms cm$^{-3}$) | $n-1$ |
|---|---|---|---|
| | Cold atom cloud | | |
| Raman selection | 1 THz | $1\times10^{10}$ | $-3.5\times10^{-10}$ |
| Bloch | 40 GHz | $2\times10^{8}$ | $-1.7\times10^{-10}$ |
| Raman measurement | 1 THz | $2\times10^{8}$ | $-7\times10^{-12}$ |
| | Background vapor | | |
| Raman | 1 THz | $8\times10^{8}$ | $-2.9\times10^{-11}$ |
| Bloch | 40 GHz | $8\times10^{8}$ | $-7.2\times10^{-10}$ |

### D. Index of refraction

In this section, we first calculate the refractive index for the Raman and Bloch beams due to both the vapor background and the atomic cloud. In a second part, using simple arguments of momentum conservation, we explain how this refractive index may induce an effect on the recoil measurement.

#### *1. Measurement of the refractive index*

For a detuning $\Delta$ larger than the natural linewidth $\Gamma$ of the atomic transition, the refractive index is given by

$$n = 1 + f\frac{3\pi}{2}\rho\frac{\Gamma}{\Delta}\left(\frac{\lambda}{2\pi}\right)^3 \tag{32}$$

where $\lambda$ is the wavelength of the transition, $\rho$ is the atomic density, and $f$ is the oscillator strength. In our case the detuning is larger than the hyperfine splitting (500 MHz), but smaller than the fine structure (7 THz); hence $f=2/3$ for the $D2$ line.

Our magneto-optical trap is loaded from a rubidium vapor. To measure the density of this vapor, we looked at the absorption of a probe beam through the cell. Because the Doppler effect is larger than the hyperfine splitting, the cross section is calculated without hyperfine splitting: $\sigma = f3\lambda^2/2\pi$. By taking into account that only 1/4 of the atoms are $^{87}$Rb, 5/8 of them are in the $F=2$ state, and that because of the Doppler effect, only a small proportion (the natural linewidth divided by the Doppler width) are resonant, we find that the total density of the background vapor is $8\times10^8$ atoms/cm$^3$.

The cold atom density is measured just after the optical molasses phase using absorption imaging on the $F=2$ to $F'=3$ transition. By integrating the attenuation of the probe beam over the cloud one can calculate the total number of atoms. Assuming a Gaussian isotropic density distribution, we obtain a density of $\rho=1.1\times10^{10}$ atoms/cm$^3$. However, we have to take into account the fact that fewer than 2% of the atoms remain after the first selection. The resulting refractive indexes are summarized in Table IV.

#### *2. Photon recoil in a dispersive medium: A simple theoretical approach*

The problem of the momentum of a photon in dispersive media is quite an old question; classically it can be expressed as the momentum of a wave packet of given energy $E$. Almost a century ago, this question lead to a controversy between Abraham [36,37], who affirmed that the photon momentum in a medium of refractive index $n$ was $E/nc$, and Minkowski [38,39], who affirmed that it should be $En/c$. Later work due to Peierls gave other values [40]. A precise calculation of the recoil induced by the reflection of a light pulse, done by Gordon [41], confirmed the Minkowski formula. This formula, applied for a quantum of light, says that the recoil of a photon of wave vector $k$ in the vacuum is $n\hbar k$. Recently, Campbell *et al.* [42] measured the recoil energy of atoms diffracted by a standing wave in an atom interferometer. The result obtained is in agreement with Minkowski formula.

This result can be obtained using the following argument. In a refractive medium of index $n$, the phase of the electric field varies as $nkx$. When the atoms interact with this field, this phase will be added to the initial phase of the atomic wave function. For a one-photon transition, this means that the momentum of the atoms increases by $n\hbar k$.

However, in the case of Bloch oscillations we know that, for each atom transferred, an incoming photon (of momentum $\hbar k$ before any interaction) will leave the medium in the opposite direction, with the same frequency and so a momentum $-\hbar k$. Consequently, for a complete Bloch oscillation, a total momentum of $2\hbar k$ will be transmitted to each atom.

As pointed out in [42], to understand the phenomenon we have to take into account the motion of the refractive medium. This can be done using the following argument. In order to calculate the recoil due to the diffraction of atoms by light, we need to calculate the phase of the light at the position of the atoms. Because we are doing a two-photon transition only the difference $\Phi=\phi_1-\phi_2$ between the phases of the two beams is involved.

Using the facts that (i) without dispersive media the phase would be $\Phi(x)=2kx$, (ii) inside the medium we have the relation $d\Phi/dx=2nk$, and (iii) at the position $\langle x\rangle$ of the center of the medium the effect due to the refractive index cancels from the first and second beams, we obtain that

$$\Phi(x) = 2(n-1)k(x-\langle x\rangle) + 2kx. \tag{33}$$

By assuming that the medium is uniform, we have $\langle x\rangle = \Sigma_i x_i/N$, where $x_i$ $(i=1,\ldots,N)$ is the position of the atoms in the dispersive medium. The function $\Phi(x)$ depends on the position of all the atoms. Consequently, when an atom is transferred, it acquires the momentum $\hbar d\Phi(x_i)/dx_i = 2n\hbar k + 2(1-n)\hbar k/N \simeq 2n\hbar k$ and each other atom $j$ $(j\neq i)$ acquires a momentum of $\hbar d\Phi(x_i)/dx_j = 2(1-n)\hbar k/N$. The approach described in this paragraph is not a full quantum approach of the refractive index, but more a mean-field approach. However, this simple calculation both leads to the result of Minkowski and respects momentum conservation.

*a. Bloch.* Let us consider the problem of Bloch oscillations in a more general way as a process transferring a fraction $\varrho$ of atoms with a two-photon transition. We obtain that the momentum of the transferred atoms is $2[n+\varrho(1-n)]\hbar k$ (each atom is transferred one time and is $\varrho N$ times in the

dispersive medium when another atom is transferred). The momentum of non transferred atoms is $2\varrho(1-n)\hbar k$.[2]

So for an efficiency of 100% there is no effect due to the refractive index. In our experiment, where the efficiency per oscillation is $\varrho > 99.95\%$, the correction due to refractive index is less than two orders of magnitude lower than the correction given by the Minkowski formula, and thus negligible.

*b. Raman*. One way to calculate the Doppler effect of a nonrelativistic atom is to consider the time derivative of the phase at the position $x(t)=vt$ of the atom: $\omega' = d\Phi(x(t),t)/dt$. To calculate the derivative of Eq. (33), we have to take into account the motion of the cloud. By assuming that the cloud is moving at a speed $v_0$, the value of the Raman frequency $\delta'$ for an atom moving at a speed $v$ is

$$\delta' = \delta - 2kv + 2(n-1)k(v_0 - v). \tag{34}$$

In the experiment, the mean velocity of the cloud at the selection is about $2Nv_r$. We select atoms in such a way that their velocity differs from this mean velocity by less than one recoil. As a consequence, the relative effect of the refractive index is of the order of $(n-1)/(2N)$ where $N \simeq 500$ is the velocity of the atoms in units of $2v_r$. With $n-1 \simeq 3\times 10^{-10}$, the effect is then completely negligible.

*c. Background vapor*. We have seen that the momentum transferred to the atoms is given by $2[1+(1-\varrho)(n-1)]\hbar k$ where $(1-\varrho)$ is the fraction of nontransferred atoms. This equation can be interpreted using the Minkowski formula in which the refractive index $n$ is replaced by the refractive index due only to nontransferred atoms $[1+(1-\varrho)(1-n)]$. Consequently, because the hot atoms from the background are out of resonance and do not perform Bloch oscillations, we have to take them into account as nontransferred atoms. This results in a relative correction of 0.75 ppb on $h/m_{\mathrm{Rb}}$.

### E. Quadratic Zeeman effect

Residual magnetic field gradients contribute to the systematics in two ways. First there is a second-order Zeeman shift of the energy levels which induces an error in the Raman velocity measurement. Second, the quadratic magnetic force modifies the atomic motion between the selection and the measurement.

#### *1. Zeeman shift in the Raman process*

As explained in Sec. II, by exchanging the direction of propagation of the two Raman beams used for the selection and the measurement of the velocity of atoms, one can change the sign of the effect due to level shifts. This assumes that between two consecutive measurements the magnetic field and the atomic position are the same. The temporal sequence being the same for the two directions of propagation, there is no reason for a systematic effect due to a temporal variation of the magnetic field. However, the position of atoms is not exactly the same because the directions of the recoils given at the first Raman transition are opposite. For the timing used in our experiment, this difference is about $\delta z = 300\ \mu$m.

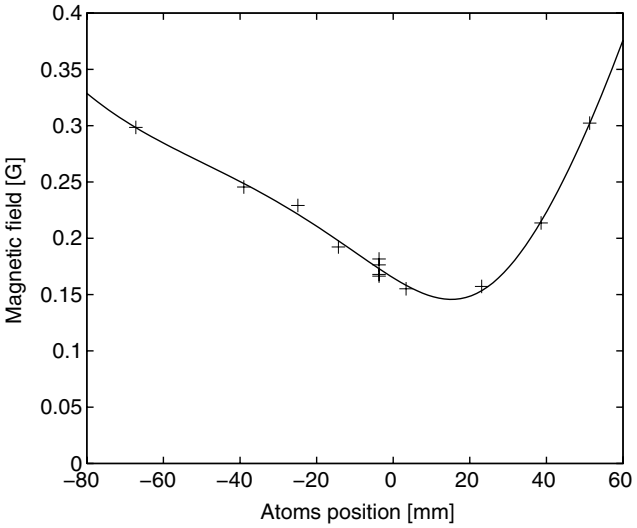


FIG. 17. Experimental determination of the magnetic field along the atomic trajectory. The zero of the atomic position corresponds to the center of the molasses.

The systematic effect arising from the position shift depends only on the gradient of the Zeeman shift ($\partial\Delta_{\mathrm{Zee}}$) at the position of the atoms at the second Raman pulse for the upper and lower trajectories. In order to measure this gradient, we perform copropagating Raman transitions. The sequence is the following. We keep the same first three steps: initial acceleration with Bloch oscillations, selection of a subrecoil velocity class, and deceleration of this velocity class. The last step is a copropagating Raman transition, between the same $|F=1,m_F=0\rangle$ and the $|F=2,m_F=0\rangle$ states—we can then measure the hyperfine splitting between the two states. This measurement includes many shifts: the Zeeman shift ($\sim$10 Hz for a magnetic field of 150 mG), the light shifts ($\sim$3.5 Hz), and the Doppler shift ($\sim$5 Hz). Indeed, for a copropagating transition, the Doppler effect, given by $(k_1-k_2)v$, is about $10^5$ times smaller than for a counterpropagating transition—but not negligible. We thus take care to make the same number of oscillations in the accelerating and decelerating processes. The final atomic velocity is then only due to the gravitational fall and can be calculated. Furthermore, both the Doppler shift and light shift can be canceled out by calculating the gradient from measurements at different positions. This is done by changing the number of Bloch oscillations.

The experiment is realized in a non-magnetically-shielded stainless steel vacuum chamber. The deduced Zeeman shift gradients (see Fig. 17) are $\partial_z\Delta^U_{\mathrm{Zee}} = 1.85\ \mathrm{Hz\ mm^{-1}}$ and $\partial_z\Delta^L_{\mathrm{Zee}} = -0.52\ \mathrm{Hz\ mm^{-1}}$ respectively, for the upper and lower trajectories.

From Eq. (25), we can estimate the correction to the value of $h/m_{\mathrm{Rb}}$:

[2]For $\varrho = 1/2$, this prediction differs by a factor of 2 from the result of Ref. [42]

$$\Delta\left(\frac{\hbar}{m_{\mathrm{Rb}}}\right)_{\mathrm{Zeeman}} = \frac{\partial_z \Delta^U_{\mathrm{Zee}} - \partial_z \Delta^L_{\mathrm{Zee}}}{8(N^{\mathrm{up}} + N^{\mathrm{down}})k_B k_R}\delta z. \tag{35}$$

The resulting relative correction on $h/m_{\mathrm{Rb}}$ for our parameters is −13.2 ppb. Taking into account the uncertainty of the magnetic field measurement, we estimate the corresponding uncertainty at 4 ppb.

#### 2. Quadratic magnetic force

The second-order Zeeman effect induces a shift in the energy levels of an atom in the magnetic field. If this magnetic field is not homogeneous, the kinetic energy of the atoms will be modified. The variation of velocity of an atom with velocity $v$ enduring a variation of energy $\Delta E$ is $\Delta v = \Delta E/mv$. We obtain that the relative correction on $h/m_{\mathrm{Rb}}$ due to this effect is

$$\frac{h}{2(N^{\mathrm{up}} + N^{\mathrm{down}})v_r}\left(\frac{\Delta^U_{\mathrm{Zee},F=1}}{mv^U_{\mathrm{sel}}} - \frac{\Delta^L_{\mathrm{Zee},F=1}}{mv^L_{\mathrm{sel}}}\right) \tag{36}$$

where $\Delta^{U/L}_{\mathrm{Zee},F=1}$ is the variation of Zeeman shift between the selection and the measurement for the upper and lower trajectories. We emphasize that only the $F=1$ hyperfine level is involved in the Bloch oscillations process.

As shown in Fig. 17, the minimum of the measured magnetic field is in the center of the chamber and therefore the induced force opposes the second Bloch acceleration. The corresponding correction to $h/m_{\mathrm{Rb}}$ is positive. For a typically measured Zeeman shift of 30 Hz, we obtain that the relative correction on $h/m_{\mathrm{Rb}}$ is 2.6 ppb. We estimate our knowledge of the magnetic field within 30% corresponding to an uncertainty of 0.8 ppb.

### F. Light shift

In the same way that the second-order Zeeman effect gives two different systematic effects, light shifts can induce an error in the Raman velocity selection and measurement and can also induce a force on atoms between Bloch oscillations.

#### 1. One-photon light shift

For atoms in $|F, m_F=0\rangle$, the light shift induced by a laser beam of intensity $I$ and detuned by $\Delta$ from the $D2$ line is, in the case where $\Delta$ is larger than the hyperfine splitting but smaller than the fine structure,

$$\delta_{\mathrm{ls}} = \frac{\Gamma^2}{8I_S}\frac{I}{\Delta} \tag{37}$$

where $\Gamma$ is the linewidth of the $5P_{3/2}$ state and $I_S$ is the saturation intensity of the $D2$ line.

However, for a Raman transition, only the differential effect from the light shift of the $|F=1, m_F=0\rangle$ and $|F=2, m_F=0\rangle$ states is important. In the case where $\Delta$ is larger than the hyperfine splitting $\omega_{\mathrm{HFS}}$ of the ground state, the differential effect is obtain by taking the derivative of Eq. (37). We obtain

$$\delta^{|F=2\rangle}_{\mathrm{ls}} - \delta^{|F=1\rangle}_{\mathrm{ls}} = -\frac{\Gamma^2 I}{8I_S}\frac{\omega_{\mathrm{HFS}}}{\Delta^2}. \tag{38}$$

The light intensity at the position of the atoms is easily measured by looking at the $\pi$ condition of a copropagating Raman transition. Indeed, the effective Raman coupling $\Omega$, in the case of a lin ⊥ lin transition, is equal to

$$\Omega = \frac{I}{I_S}\frac{\Gamma^2}{16|\Delta|}. \tag{39}$$

Combining Eqs. (38) and (39), and using the fact that we have to add the light shift of three beams (one of the Raman beams is retroreflected), we obtain that

$$\delta^{|F=2\rangle}_{\mathrm{ls}} - \delta^{|F=1\rangle}_{\mathrm{ls}} = -\frac{6\pi}{\tau}\frac{\omega_{\mathrm{HFS}}}{|\Delta|}. \tag{40}$$

With our parameters, one can calculate that the light shift will shift the transition by 75 Hz—leading to a change in velocity by about $5\times10^{-3}v_r$. This effect is important. However, one can expect to cancel it in many ways: between the selection and measurement (constant effect is canceled), upper and lower trajectories (time-dependent effect is then canceled), and by reversing the direction of propagation of the Raman beam (position-dependent effect is canceled). The inversion of the direction of the Raman beams, which should result in the cancellation of level shifts (up to a systematic shift in the position of atoms) does not work well for light shifts, because of a possible systematic change in the intensity of light when the direction of propagation is changed. Thus, we do not compensate either the effect resulting from spatial variations of light or the effect caused by the spread of the atomic cloud and the finite size of the laser beam. The intensity at the measurement will be, on average, less than the intensity at the selection.

Let us denote by $\Delta^0_{\mathrm{ls}}$ the light shift for the selection, by $\xi$ a parameter such that the residual light shift due to the spread of the cloud is $\Delta^0_{\mathrm{ls}}(1-\xi)$ at the measurement, by $R$ a typical length for the variation of intensity, and by $\beta$ the relative difference of intensity between the Raman beams when we exchange their direction of propagation.

The correction to apply to $h/m_{\mathrm{Rb}}$ is then

$$\frac{\beta}{R}\frac{\Delta^0_{\mathrm{ls}}(z^U_{\mathrm{sel}} - z^L_{\mathrm{sel}}) - \Delta^0_{\mathrm{ls}}(1-\xi)(z^U_{\mathrm{meas}} - z^L_{\mathrm{meas}})}{8(N^{\mathrm{up}} + N^{\mathrm{down}})k_R k_B} \tag{41}$$

where $z^{U/L}_{\mathrm{sel/meas}}$ are the positions of atoms during the selection and measurement for the upwards and downward trajectories (see Fig. 16).

We measure $\beta < 10\%$ and estimate $R \gtrsim 10$ m. Consequently, the effect, of the order of $2\times10^{-10}$ for $h/m_{\mathrm{Rb}}$, is negligible and we decide not to apply any correction.

#### 2. Two-photon light shift

There is a two-photon light shift induced by the copropagating Raman beams coming out of the same fiber (afterward one of them will be retroreflected in order to form the counterpropagating beam). The experiment is based on the fact that, because we are addressing moving atoms, only the velocity-selective transition is resonant. However, the copropagating one will induce a light shift given by

$$\delta_{\mathrm{ls\ 2ph}} = -\frac{\Omega^2}{2\delta}. \tag{42}$$

This light shift, inversely proportional to the detuning $\delta$ of the transition—and thus to the velocity of atoms—is larger during the second Raman pulse. It does not cancel between the upward and downward trajectories because we are not using a totally symmetric scheme (due especially to gravity and a different number of transmitted recoils). Finally, we obtain that the relative effect on $h/m_{\mathrm{Rb}}$ is

$$\frac{\Omega^2}{2}\frac{(\delta^U_{\mathrm{sel}})^{-1} - (\delta^U_{\mathrm{meas}})^{-1} - (\delta^L_{\mathrm{sel}})^{-1} + (\delta^L_{\mathrm{meas}})^{-1}}{\delta^U_{\mathrm{sel}} - \delta^U_{\mathrm{meas}} - \delta^L_{\mathrm{sel}} + \delta^L_{\mathrm{meas}}}. \tag{43}$$

With our experimental parameters, the corresponding correction to $h/m_{\mathrm{Rb}}$ is 1 ppb with an uncertainty of 0.4 ppb.

#### *3. Light shift gradient during Bloch oscillation*

Another important systematic effect induced by a spatial variation of the light intensity is the dipolar electric force. This force modifies the atomic velocity during Bloch oscillations. A rough calculation based on light shifts considering about $U_0 = 100E_r$ and a typical length for the variation of light shift $R = 10$ m leads to a force $F = U_0/R$ giving an acceleration of $3\times10^{-5}v_r\ \mathrm{ms}^{-1}$. This effect is then nonnegligible.

However, this force cannot be calculated by adding the force due to the gradient of each beam: we have to take into account both the interference of the lasers and the fact that the wave function of atoms is not uniform. In particular, in the case of a deep blue-detuned lattice, atoms are located in spatial positions where the light intensity is minimal. The effect is then highly reduced. Furthermore, only the spatial variation of this force is important, because any constant force (such as gravity) will cancel out from the upper and lower trajectories.

To evaluate this effect, we calculate the energy of an atom in the fundamental band of the lattice as a function of its position. The energy level in the tight-binding limit is then given by

$$U = \frac{U_0}{4}\frac{(\mathcal{E}_U - \mathcal{E}_D)^2}{\mathcal{E}_U\mathcal{E}_D} + \sqrt{U_0 E_r} \tag{44}$$

where $\mathcal{E}_{U/D}$ are the amplitudes of the electromagnetic field of the upward and downward propagating beams which form the optical lattice. The first term of Eq. (44) corresponds to the minimum energy in the lattice potential and the second term is the energy of the harmonic oscillator in the potential well. It is important to notice that this formula is valid only for a blue-detuned lattice. This energy shift induces a force $F = -\partial U/\partial z$.

In the tight-binding limit, because $U_0 \gg 16E_r$, the contribution of the second term of Eq. (44) is small. As mentioned above, all constant forces cancel out between the upper and lower trajectories and only the gradient of the force $(\partial/\partial z)F(z)$ contributes to the systematics. By neglecting the second term in Eq. (44), we obtain that

TABLE V. Error budget on the determination of $h/m_{\mathrm{Rb}}$ (systematic effect and relative uncertainty in ppb).

| Source | Correction (ppb) | Relative uncertainty (ppb) |
|---|---|---|
| Laser frequencies | | 1.6 |
| Beams alignment | 4 | 4 |
| Wave-front curvature and Gouy phase | 16.4 | 8 |
| Second-order Zeeman effect | −13.2 | 4 |
| Quadratic magnetic force | 2.6 | 0.8 |
| Gravity gradient | 0.36 | 0.04 |
| Light shift (one-photon transition) | | 0.4 |
| Light shift (two-photon transition) | 1.0 | 0.4 |
| Light shift (Bloch oscillation) | −0.92 | 0.4 |
| Index of refraction of atomic cloud | | 0.6 |
| Index of refraction of background vapor | 0.75 | 0.6 |
| Global systematic effects | 10.98 | 10.0 |

$$\frac{\partial F(z)}{\partial z} = 2\frac{U_0}{\kappa}\left[(\kappa-1)\left(\frac{\gamma_U}{R_U^2} - \kappa\frac{\gamma_D}{R_D^2}\right) - \left(\frac{1}{R_U} - \frac{\kappa}{R_D}\right)^2\right] \tag{45}$$

where $\kappa = \mathcal{E}_D/\mathcal{E}_U$, $R_{U/D}$ are the curvature radius of the upward and downward propagating beams, and $\gamma_{U/D}$ are dimensionless factors given by the relations

$$\gamma_{U/D} = 2 - \left(\frac{\lambda R_{U/D}}{\pi w^2_{U/D}}\right)^2. \tag{46}$$

Because our measurement was done with beams of different curvature radius, the force gradient is not null, even for beams of equal intensity ($\kappa = 1$). Using the parameters of Table III, we obtain a systematic correction on $h/m_{\mathrm{Rb}}$ of $-9.2\times10^{-10}$. The uncertainty, coming mainly from the uncertainty on the wave-front curvature, is $4\times10^{-10}$. We did not take this effect into account in our previous publication [20]. Therefore the value of the fine-structure constant $\alpha$ is slightly different from that published in this reference.

### G. Final results and uncertainty budget

We summarize in Table V the different systematic effects and their contributions to the uncertainty on the determination of the ratio $h/m_{\mathrm{Rb}}$. All the uncertainties are added in quadrature. The largest uncertainty comes from the laser geometric parameters (wave-front curvature, waist, alignment) (9 ppb). All these parameters were measured *a posteriori*. The contribution of the magnetic field to the systematics was experimentally determined by mapping the magnetic field gradient experienced by the atoms. Those uncertainties can be reduced by using appropriate techniques. More fundamental uncertainties come from the different light shifts in the experiment (0.7 ppb). Finally, concerning the index of refraction effect, we have assumed a conservative uncertainty of 0.85 ppb derived from the calculation of the Bloch and Raman wavelengths in the medium.

TABLE VI. Constants used for the determination of $\alpha$ from $h/m_{\mathrm{Rb}}$.

| | Value | Relative uncertainty (ppb) |
|---|---|---|
| Rydberg constant [1] | 10 973 731.568 525(73) $\mathrm{m}^{-1}$ | 0.0006 |
| Rubidium mass [19] | 86.909 180 520(15) amu | 0.2 |
| Electron mass [1] | 5.485 799 0945(24) $10^{-4}$amu | 0.44 |

Table VI shows the different constants used for the determination of $\alpha$ from our measurement. Their uncertainties are negligible. Taking into account the corrections, we obtain that

$$\frac{h}{m_{\mathrm{Rb}}} = 4.591\ 359\ 29(6) \times 10^{-9}\ \mathrm{m}^2\ \mathrm{s}^{-1} \quad [1.3 \times 10^{-8}], \tag{47}$$

$$\alpha^{-1} = 137.035\ 998\ 84(91) \quad [6.7 \times 10^{-9}]. \tag{48}$$

## VII. CONCLUSION AND PROSPECTS

Thanks to the high efficiency of the Bloch oscillations process (99.97% per recoil), we are able to transfer to the atoms about 900 photon momenta. This method combined with a precise velocity sensor leads to a measurement of the ratio $h/m_{\mathrm{Rb}}$ with a relative uncertainty of $1.3\times10^{-8}$. This noninterferometric measurement achieves a precision comparable to the best measurement provided by an atomic interferometry experiment [2]. A comparison of our determination of $\alpha$ with other determinations is presented in Fig. 18. Except for the more recent value of $\alpha$ obtained from the measurement of $a_e$ [5], all the values used for this comparison come from the last CODATA report. This determination of $\alpha$ with an uncertainty below 10 ppb will increase the confidence on the $\alpha$ value at this level of uncertainty.

We plan several improvements in order to achieve a 1 ppb level uncertainty on $\alpha$. The statistical uncertainty of our current measurement (4.4 ppb) arises from the signal-to-noise ratio of the velocity sensor. We expect to improve this ratio by a factor of 4, first by increasing significantly the initial density of atoms in velocity space, and second by implementing a vibration isolation platform in our experimental setup. On the other hand, by increasing the number of recoils transmitted to the atoms (using a much larger cell and a more powerful laser), we plan to reduce the statistical uncertainty significantly below 1 ppb.

We need also to control more carefully the systematic effects (5 ppb, in the current measurement). For this purpose, we consider several enhancements: (i) A better control of the geometrical parameters of the Raman and Bloch laser beams will allow us to reduce the uncertainty coming from the wave-front curvature. (ii) A magnetic shielding of the vacuum chamber, associated with the differential measurement currently used to bring down systematics, will probably reduce by one order of magnitude effects due to the magnetic field. (iii) Laser frequency stabilization and measurement can easily be improved to neglect the associated systematic effect at the ppb level. (iv) A better determination and control of experimental parameters involved in the light shift and the refractive index will be required to reduce the uncertainty on their estimations.

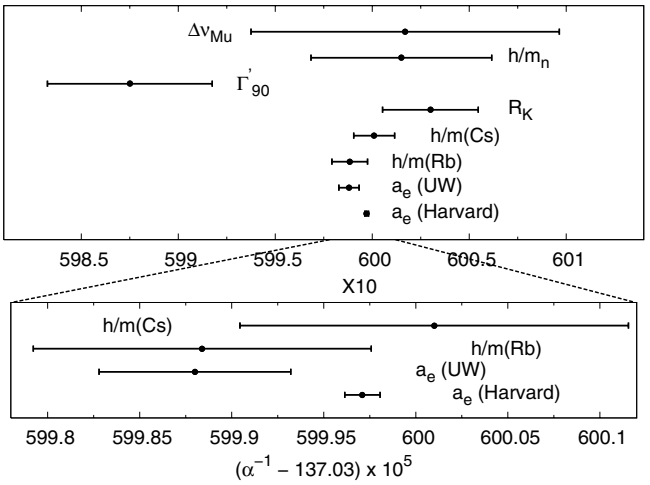


FIG. 18. Comparison of our measurement $[h/m(\mathrm{Rb})]$ with the measurements used for the 2002 CODATA adjustment [1] and the measurement of Ref. [5] (Harvard).

Furthermore, improvements in the statistical uncertainty (due to the reduction of integration time) may allow us to place experimental error bars on systematic effects by making measurements with different parameters. These major improvements should lead to a measurement of $\alpha$ below the ppb level.

A new measurement of the fine-structure constant at the ppb level would have an important consequence not only in metrology but also in fundamental physics. Indeed, with the recent 0.7 ppb determination of $\alpha$ from the measurement of $a_e$, such a determination, which is almost independent of QED, would lead to an unprecedented test of QED and of the internal structure of the electron [5].

## ACKNOWLEDGMENTS

We wish to thank A. Clairon, C. Salomon, S. Reynaud, and P. Wolf for valuable discussions. This experiment is supported in part by the Laboratoire National de Métrologie et d'Essais (Ex. Bureau National de Métrologie) (Contract No. 033006) and by the Région Ile de France (Contract No. SESAME E1220). The work of E.d.M. is supported by IFRAF (Institut Francilien de Recherches sur les Atomes Froids).

[1] P. Mohr and B. N. Taylor, Rev. Mod. Phys. **77**, 1 (2005).
[2] A. Wicht *et al.*, Phys. Scr., T **102**, 82 (2002).
[3] B. Odom, D. Hanneke, B. D'Urso, and G. Gabrielse, Phys. Rev. Lett. **97**, 030801 (2006).
[4] T. Kinoshita and M. Nio, Phys. Rev. D **73**, 013003 (2006).
[5] G. Gabrielse, D. Hanneke, T. Kinoshita, M. Nio, and B. Odom, Phys. Rev. Lett. **97**, 030802 (2006).
[6] C. J. Bordé, Philos. Trans. R. Soc. London, Ser. A **363**, 2177 (2005).
[7] I. M. Mills, P. J. Mohr, T. J. Quinn, B. N. Taylor, and E. R. Willams, Metrologia **43**, 227 (2006).
[8] A. Jeffery *et al.*, Metrologia **35**, 83 (1998).
[9] S. Chu, C. Cohen-Tannoudji, and W. D. Phillips, Rev. Mod. Phys. **70**, 685 (1998).
[10] G. Santarelli *et al.*, Phys. Rev. Lett. **82**, 4619 (1999).
[11] C. W. Oates, K. R. Vogel, and J. L. Hall, Phys. Rev. Lett. **76**, 2866 (1996).
[12] A. Peters, K. Y. Chung, and S. Chu, Metrologia **38**, 25 (2001).
[13] T. L. Gustavson, P. Bouyer, and M. A. Kasevich, Phys. Rev. Lett. **78**, 2046 (1997).
[14] D. S. Weiss, B. C. Young, and S. Chu, Phys. Rev. Lett. **70**, 2706 (1992).
[15] B. Taylor, Metrologia **31**, 181 (1994).
[16] Th. Udem *et al.*, Phys. Rev. Lett. **79**, 2646 (1997).
[17] C. Schwob *et al.*, Phys. Rev. Lett. **82**, 4960 (1999).
[18] T. Beir *et al.*, Phys. Rev. Lett. **88**, 011603 (2001).
[19] M. P. Bradley *et al.*, Phys. Rev. Lett. **83**, 4510 (1999).
[20] P. Cladé *et al.*, Phys. Rev. Lett. **96**, 033001 (2006).
[21] R. Battesti *et al.*, Phys. Rev. Lett. **92**, 253001 (2004).
[22] P. D. Lett, R. N. Watts, C. I. Westbrook, W. D. Phillips, P. L. Gould, and H. J. Metcalf, Phys. Rev. Lett. **61**, 169 (1988).
[23] P. Cladé, S. Guellati-Khélifa, C. Schwob, F. Nez, L. Julien, and F. Biraben, Eur. Phys. J. D **33**, 173 (2005).
[24] M. Ben Dahan *et al.*, Phys. Rev. Lett. **76**, 4508 (1996).
[25] F. Bloch, Z. Phys. **52**, 555 (1928).
[26] G. H. Wannier, Phys. Rev. **52**, 191 (1937).
[27] P. Cladé, S. Guellati-Khélifa, C. Schwob, F. Nez, L. Julien, and F. Biraben, Europhys. Lett. **71**, 730 (2005).
[28] G. Morigi, J. Eschner, J. I. Cirac, and P. Zoller, Phys. Rev. A **59**, 3797 (1999).
[29] D. Touahri *et al.*, Opt. Commun. **133**, 471 (1997).
[30] B. de Beauvoir, F. Nez, L. Hilico, L. Julien, F. Biraben, B. Cagnac, J. J. Zondy, D. Touahri, O. Acef and A. Clairon, Eur. Phys. J. D **1**, 227 (1998).
[31] B. De Beauvoir, C. Schwob, O. Acef, L. Jozefowski, L. Hilico, F. Nez, L. Julien, A. Clairon, and F. Biraben, Eur. Phys. J. D **12**, 61 (2000).
[32] A. Clairon *et al.*, IEEE Trans. Instrum. Meas. **44**, 128 (1995).
[33] A. Wicht, E. Sarajlic, J. M. Hensley, and S. Chu, Phys. Rev. A **72**, 023602 (2005).
[34] A. Ashkin, J. M. Dziedzic, J. E. Bjorkholm, and S. Chu, Opt. Lett. **11**, 288 (1986).
[35] H. Kogelnik and T. Li, Appl. Opt. **5**, 1550 (1966).
[36] M. Abraham, Rend. Circ. Mat. Palermo **28**, 1 (1909).
[37] M. Abraham, Rend. Circ. Mat. Palermo **30**, 33 (1910).
[38] H. Minkowski, Nachr. Ges. Wiss. Goettingen, Math.-Phys. Kl. 53 (1908).
[39] H. Minkowski, Math. Ann. **68**, 472 (1910).
[40] R. Peierls, in Proceedings of the Scuola Normale Superiore, Pisa, 1987 (unpublished), p. 187.
[41] J. P. Gordon, Phys. Rev. A **8**, 14 (1973).
[42] G. K. Campbell *et al.*, Phys. Rev. Lett. **94**, 170403 (2005).